

CACTUSDB: Unlock Co-Optimization Opportunities for SQL and AI/ML Inferences

(Accepted to ICDE 2026 as a full research paper)

Lixi Zhou^a, Kanchan Chowdhury^a, Lulu Xie^a, Jaykumar Tandel^a,
Hong Guan^a, Zhiwei Fan^b, Xinwei Fu^c, Jia Zou^a

^a Arizona State University, ^b Meta, ^c Amazon

Abstract—There is a growing demand for supporting *inference queries* that combine Structured Query Language (SQL) and Artificial Intelligence / Machine Learning (AI/ML) model inferences in database systems, to avoid data denormalization and transfer, facilitate management, and alleviate privacy concerns. Co-optimization techniques for executing inference queries in database systems without accuracy loss fall into four categories: (O1) Relational algebra optimization treating AI/ML models as black-box user-defined functions (UDFs); (O2) Factorized AI/ML inferences; (O3) Tensor-relational transformation; and (O4) General cross-optimization techniques. However, we found none of the existing database systems support all these techniques simultaneously, resulting in suboptimal performance. In this work, we identify two key challenges to address the above problem: (1) the difficulty of unifying all co-optimization techniques that involve disparate data and computation abstractions in one system; and (2) the lack of an optimizer that can effectively explore the exponential search space. To address these challenges, we present CACTUSDB, a novel system built atop Velox - a high-performance, UDF-centric database engine, open-sourced by Meta. CACTUSDB features a three-level Intermediate Representations (IR) that supports relational operators, expression operators, and ML functions to enable flexible optimization of arbitrary sub-computations. Additionally, we propose a novel Monte-Carlo Tree Search (MCTS)-based optimizer with query embedding, co-designed with our unique three-level IR, enabling shared and reusable optimization knowledge across different queries. Evaluation of 12 representative inference workloads and 2,000 randomly generated inference queries on well-known datasets, such as MovieLens and TPCx-AI, shows that CACTUSDB achieves up to 441× speedup compared to alternative systems.

Index Terms—database, machine learning, query optimization

I. INTRODUCTION

It is important to nest Artificial Intelligence / Machine Learning (AI/ML) inferences and Structured Query Language (SQL) queries to drive high-value insights from relational data, e.g., to generate personalized product recommendations [1]–[3] based on preprocessed customer profiles and online shopping records through `join`, `filter`, and `project` nested with AI/ML model inferences, to obtain statistics about credit card transactions that are predicted as fraud [4], through `aggregate`, `join`, and `filter`, nested with inferences. A broad class of works on using AI to enhance database systems further strengthens such demands [5]–[8]. Therefore, a recent trend of supporting SQL queries nested with AI/ML inference functions within database systems has emerged [9]–[19]. This approach eliminates the need to transfer data from databases to ML systems. It not only reduces latency in workloads where

data transfer becomes a bottleneck [20] but also alleviates privacy concerns [21] and operational overhead [22], [23].

Most importantly, having SQL and ML running in the same system will unlock co-optimization opportunities and reduce execution costs without affecting accuracy. We summarize the co-optimization techniques into four categories:

(O1) Relational algebra optimization. An inference query may involve AI/ML-based `filters` that invoke AI/ML models on the input data to return a Boolean value, such as `predict(movieFeatures)=True`. Based on the estimated costs of the AI/ML models and the selectivity of the predicates, the system can push down such `filters` through `join`, without knowing the internal logic of the AI/ML models to avoid redundant computations. Similar techniques include pushing down AI/ML-based `project` operators, reordering two consecutive customized `filters`, and merging multiple consecutive AI/ML-based `filter/projects` into one. User-Defined Function (UDF)-centric systems [10], [24] and systems with extended operators [9] support some of these techniques. **(O2) Factorized inference.** An AI workflow (e.g., a two-tower recommendation model [25]) may process features that are joined from multiple tables. These workflows/functions can often be factorized into multiple independent functions, each processing features from a separate table. Then, each factorized computation can be pushed down through the `join` to its corresponding table to avoid redundant computations. The idea was extended from several works [16], [26]–[28] in the context of factorized ML [26], [29].

(O3) Tensor-relational transformation. Model parameters (e.g., weight matrices or decision trees) can be stored as relational tables, and inference can be rewritten into relational operators such as `join/project/aggregate` over these tables. This makes inference transparent to the database engine and allows it to scale via buffer-pool management and pipelined, parallel execution, even when model parameters are too large to fit in memory [30]–[35].

(O4) Data-model and cross-library optimization techniques. Seeing AI/ML as a white box, there are more cross-optimization techniques, e.g., fusing AI/ML operators from different libraries [36], [37], pruning nodes from decision forest models based on the relational predicates applied to the data to be inferred, and pruning attributes from datasets based on model logic [38]. Another co-optimization technique in this category is to replace ML operators on dense tensors with operators optimized for sparse tensors, assuming that the database is

aware that the input data is sparse [39].

The Problem and the Challenges. As detailed in Sec. VI, most of the existing DB-for-AI systems [9]–[11], [24], [27], [29]–[31], [38], [40], [41] *cannot* adaptively exploit diverse optimization techniques in O1-O4 for different sub-computations, and thus they will miss the optimization opportunities brought by combining techniques from more than one category, leading to sub-optimal query latency. The research challenges include: **Challenge 1. Difficulties in unifying all co-optimization techniques in one system.** Each category of co-optimization techniques relies on a different data/computational abstraction, cost model, and transformation logic. Relational algebra optimizations (O1) rely on classical query planning rules and cost models based on the statistics and selectivity of opaque UDFs. Factorizing an ML function across joins (O2) requires analyzing the internal structure of the UDFs and the data schema together. Tensor-relational rewrites (O3) not only require analyzing the internal logic of UDFs but also converting tensor data into collections of tensor blocks for relational processing. Data-model and cross-library optimization (O4) demand reasoning about both data layout and model internals. Existing intermediate representations and systems typically support only limited combinations of these abstractions and lack mechanisms to express all required cross-level optimizations in a coherent, cost-aware way. **Challenge 2. Massive Search Space.** Our three-level Intermediate Representations (IR) has enabled full co-optimization opportunities, which enlarged the search space. Supposing there are n atomic ML functions, each function has two options, converting to relational operators or not, which leads to 2^n optimization plans in the O3 category. Then, applying O3 techniques brings new relational operators, which will expand O1’s search space. In O4, depending on how n consecutive atomic ML functions should be fused, we will have 2^{n-1} plans. If an atomic ML function is not fused with other functions, it may bring new optimization opportunities in O2 and O3. It is essential to explore IR-optimizer co-design to effectively manage this expanded search space.

To address these challenges, we present CACTUSDB, a novel UDF-centric system with:

(1) **A Three-Level IR (Sec. III).** To address the first challenge, we advocate a three-level IR on top of the approach combining relational and linear algebra, to capture computation at different layers. The top level consists of relational operators nested with opaque user-defined expressions. At the middle level, each opaque expression at the top level is lowered to analyzable tree structures, in which each node is either an expression operator or an opaque expression. At the bottom level, each opaque expression from the middle-level IR is (optionally) described as a computational graph of ML or UDF functions. We leverage the underlying Velox system for query/expression parsing, vectorization, and physical optimization.

(2) **A Novel Reusable MCTS Optimizer (Sec. IV).** Today’s cost-based query optimizers increasingly adopt the MCTS for efficiently exploring large search spaces, balancing exploitation and exploration via the Upper Confidence Bound (UCB) mechanism [42], and integrating with diverse models. However,

existing MCTS-based query optimizers [43]–[46] need to build a search tree from scratch for each query, as each has distinct states (query plans) and action spaces (rewrite rules), making reuse of MCTS tree challenging. We address this by combining query embeddings with MCTS to form a universal state space. Our embedding design aligns with the three-level IR, while the action space consists of co-optimization rules (O1–O4).

(3) **Implementation and A Comprehensive Evaluation (Sec. V).** We implemented CACTUSDB¹ on top of Meta’s open-sourced Velox database engine [47]. We further evaluated our system on several benchmarks, including (1) realistic recommendation queries on MovieLens dataset [48], [49] (2) TPCx-AI workloads [50], and (3) analytics workloads on three real-world datasets - Credit Card [51], Expedia [52], and Flights [52]. For the MovieLens and TPCx-AI workloads, we designed ten representative query templates for each by extracting and generalizing patterns from the most popular Kaggle notebooks. We then sampled 2,000 queries based on these templates for evaluation. We observed up to $441\times$ speedup using CACTUSDB compared to baseline systems.

II. BACKGROUND

A. SQL-ML Co-Optimization

First, without loss of generality, we assume that pure relational algebra optimization, such as join reorder and the push-down of simple predicates and projections that do not involve ML, is applied before performing co-optimization, and typical database physical optimization, e.g., join algorithm selection, is applied after co-optimization.

Then, we categorize (non-approximate) SQL-ML co-optimization techniques into four main classes, O1–O4, each defined by its distinct data abstraction (particularly how model parameters are represented) and computation abstraction.

O1. Relational Algebra Optimization [9], [11], [24], [53]. O1 performs optimization at the relational algebra level. The *computation abstraction* consists of standard relational operators such as `filter`, `project`, `join`, `crossJoin`, and `aggregate`. AI/ML inference is encapsulated within user-defined expressions and treated as opaque functions. The *data abstraction* consists solely of relations; model parameters (e.g., weight tensors) are not exposed to the optimizer. Despite this opacity, the optimizer can reduce the *number* and *placement* of AI/ML invocations by rewriting the relational query plan. Representative co-optimization rules in this category (R1-1 to R1-4) are summarized below. Rules in this category preserve relational algebra equivalence provided that AI/ML models used within UDFs are deterministic.

R1-1 filter Reorder. Reordering `filter` operators, including those containing user-defined expressions, preserves query equivalence. Ordering filters by selectivity reduces intermediate result sizes.

R1-2 filter Pushdown. Pushes a `filter` down through a `join` to avoid redundant inference over high-cardinality join outputs that usually contain repeated tuples.

¹Open source at: <https://github.com/asu-cactus/cactusdb>

R1-3 project Pushdown. Pushes `project` operators, including those invoking ML inference, below `joins` to eliminate unnecessary computation.

R1-4 Operator Merge/Split. Multiple `filter` or `project` operators over the same relation can be merged into a single operator; splitting is the inverse transformation.

O2. Factorized Inference (derived from factorized ML [16], [27]–[29]). O2 extends relational optimization by exposing a richer computation abstraction that includes relational operators, linear algebra primitives, and a restricted set of factorizable ML operators (e.g., vector–matrix multiplication). The *data abstraction* explicitly exposes model parameters as factorizable objects, enabling the optimizer to reason about shared computation across joined relations. Representative co-optimization techniques are illustrated below.

R2-1 Linear Algebra Operator Factorization [27]–[29]. Let $S(Y, \mathbf{X}_S, FK)$ and $R(RID, \mathbf{X}_R)$ be two relations with feature vectors \mathbf{X}_S and \mathbf{X}_R . Joining on $S.FK = R.RID$ produces $T(Y, \mathbf{X})$, where $\mathbf{X} = [\mathbf{X}_S, \mathbf{X}_R]$. Consider a linear inference operation that computes $w^\top x^\top$ for each $x \in T.X$. Since the join replicates feature vectors from S and R across many output tuples, naively evaluating $w^\top x^\top$ on T incurs redundant computation. By partitioning the weight matrix as $w = [w_S, w_R]$, the computation can be rewritten as $w_S^\top x_S^\top + w_R^\top x_R^\top$. This factorization enables pushing $w_S^\top x_S^\top$ to S and $w_R^\top x_R^\top$ to R prior to the join, and combining the results by addition after the join, thereby eliminating repeated matrix multiplications. An example is shown in Fig. 1.

Beyond linear models, equivalent factorization strategies have been developed for linear regression, k -means clustering, decision trees, and gradient-boosted trees (e.g., Morpheus [28], LMFAO [29], JoinBoost [54], InferF [16]), with formal equivalence proofs provided in these works.

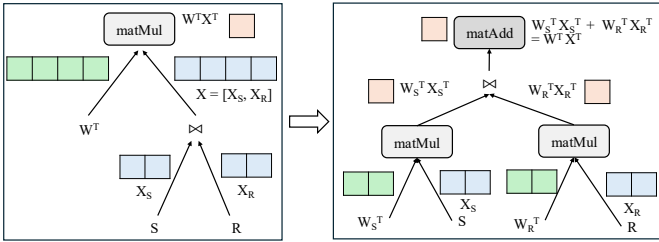


Fig. 1: Example Factorization of Matrix Multiplication (R2-1)

O3. Tensor-Relational Transformation. The computation abstraction: all AI/ML models are transformed into a limited set of tensor-relational operators [30], such as `aggregate`, `crossJoin`, `filter`, `project`, `rekey`, `tile`, `concat`, all processing tensor relations. In the *data abstraction*, the model parameters must be transformed into tensor relations. Example co-optimization techniques include:

R3-1 Linear algebra operators transformed to relational operators [30], [55]–[58]. Consider computing $Y = xW^\top$ for N input feature vectors, where x represents a row from the input table (i.e., a feature vector), and the weight matrix W is too large to fit in memory. R3-1 stores W as a *tensor relation* of column blocks, $\widetilde{W}(colld, wTile)$, and rewrites inference into a simple relational pipeline: `crossJoin`→`project`, producing block

outputs $B(rowId, colld, yBlock)$. At runtime, the DB scans \widetilde{W} one tile at a time. For each $wTile$ loaded into the buffer pool, it computes the corresponding output block $yBlock := x \cdot wTile^\top$ for all rows, emits B , and then loads the next block. Finally, it assembles each output vector by concatenating $yBlock$ blocks per $rowId$. The process is illustrated in Fig. 2. As described in Tensor Relational Algebra (TRA) [30], other linear algebra computations can also be represented in relational algebra.

R3-2 Decision Forest to relational operators [20]. A decision forest model, like XGBoost or lightGBM, is stored as $DF(treeId : INT, trees : DecisionTreeObject)$. Applying the model DF to each $x \in T.X$, could be transformed into relational processing by first performing a `crossJoin` of T and DF . Then a `project` is applied to each joined pair of $(x \in T.X, t \in DF.trees)$ to run $t.predict(x)$. The prediction results are aggregated to obtain the final prediction, e.g., via majority voting or a sigmoid function.

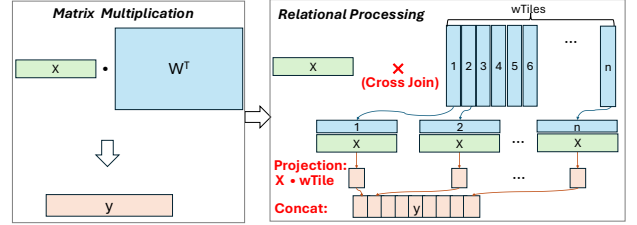


Fig. 2: Example of MatMul to Relational Processing (R3-1)

The O3 transformations scale to AI/ML models that involve a large volume of parameters, by blocking the parameters so that each time only a few blocks need to be loaded into the memory (via buffer pool management). The formal proof for the equivalence of transformation rules in O3 was provided in prior work [30].

O4. Data–Model Cross Optimization [36], [38], [59], [60]. O4 removes the abstraction boundary between data processing and model execution. The *computation abstraction* spans relational operators, linear algebra primitives, and AI/ML operators, while the *data abstraction* jointly includes relations and tensor objects (e.g., model parameters and intermediate activations). By explicitly exposing AI/ML operators and tensor data, the optimizer can jointly reason about data access patterns, operator structure, and execution strategies across the data–model boundary. Representative optimization techniques are summarized below.

R4-1 Operator Fusion and Split. Consecutive AI/ML operators can be fused into a single composite operator to reduce materialization and invocation overhead. For example, a sequence of matrix multiplication, matrix addition, and activation (e.g., `matMul` → `matAdd` → `sigmoid`) can be replaced with a single dense-layer operator from a deep learning library. Conversely, a monolithic UDF can be split into finer-grained operators, enabling selective application of factorization or parameter-aware optimizations (e.g., O2 and O3) to sub-computations.

R4-2 AI/ML Library Replacement. The physical implementation of an AI/ML operator can be substituted with alternative library backends based on hardware characteristics or data properties. For instance, `matMul` may be executed using CPU, GPU, sparse, or dense kernels. Similarly, a `conv2D` operator can be rewritten as `matMul` via spatial reorganization of inputs and filters [61]–[63]. Other techniques in this category include data-induced model optimization [38] and inference batch size optimization [64].

The correctness of the above rules (i.e., transformation equivalence) relies on the functional equivalence of alternative physical implementations of the same logical operators. In

practice, systems ensure equivalence through library guarantees and empirical validation.

In this paper, we advocate supporting all categories of optimization techniques within a unified database system. Such a design allows different sub-computations to operate under different data abstractions and co-optimization regimes, thereby enabling optimization opportunities that are inaccessible when techniques are applied in isolation. For example, after applying operator splitting (R4-1) to decompose a dense-layer UDF into finer-grained operators, linear algebra primitives such as `matMul` become explicitly visible to the optimizer, making them eligible for factorization- and parameter-aware optimizations (e.g., R2-1 and R3-1).

III. THREE-LEVEL IR

In this section, we introduce our data and computation abstractions and describe our three-level IR design and usage.

A. Flexible Data Abstraction

We abstract features and model variables as follows:

Feature Vectors are extracted from relations and stored alongside other attributes, denoted as $F(A_1 : Type_1, \dots, A_l : Type_l, \mathbf{V} : \text{vec} \in \mathbb{R}^d)$, where A_i is an attribute of type $Type_i$, and \mathbf{V} represents the stored feature vectors. If \mathbf{V} concatenates m vectors V_1, \dots, V_m , where V_1, \dots, V_m are from datasets D_1, \dots, D_m , respectively, we define $\mathbf{V} \equiv [V_1, \dots, V_m]$.

Model Parameters are variables of ML functions, which are created when models are loaded into CACTUSDB. A variable can be a tensor (deep learning), a tree collection (decision forest), or other types of parameters. A variable could be stored as a relation. For example, a d -dimensional weight tensor W_i can be stored as a relation $P_i(dim_1 : INT, \dots, dim_d : INT, block : \text{vec} \in \mathbb{R}^{k_1 \times \dots \times k_d})$, where each tuple represents a d -dimensional tensor block indexed by dim_1, \dots, dim_d , with the block data of shape $k_1 \times \dots \times k_d$ flattened as an array in the column `block`. Similarly, a decision forest can be stored as a relation $DF(TreeId : INT, TreeObj : TreeType)$, where each tuple represents a tree object indexed by `TreeId`. To enable efficient conversion, CACTUSDB selectively materializes model variables as relations during loading if their size exceeds a threshold (typically half the available memory).

B. Three-Level Computation Abstraction

CACTUSDB supports three types of operators:

Relational Operators. CACTUSDB supports most relational operators such as `filter`, `project`, `join`, `crossJoin`, `union`, `aggregate`, and `expand` (i.e., similar to `flatMap`). Each such operator processes a relation, such as F, P_i, DF .

Expression. Most relational operators should be customized by expressions, which are in the form of analyzable tree structures. A tree node can either be an opaque expression or an expression operator, such as arithmetic ($+$, $-$, $*$, $/$), comparison ($>$, $<$, $=$, \neq), bit (e.g., \wedge , \vee), relation (e.g., AND/OR), conditional (e.g., IF/THEN/ELSE and SWITCH), and function call (e.g., CALLFUNC) operators. Each expression operates on one or multiple columns, e.g., $A_i, \mathbf{V}, dim_j, block$.

ML Functions. In CACTUSDB, we have implemented a set of ML functions. An ML function is a specialized Velox UDF. Each ML function class has an `apply` method, which takes a batch of vectors or tensor blocks as input to facilitate the use of SIMD instructions and reduce virtual function call overheads. Although this work focuses on CPU-based database systems, GPU acceleration can also be enabled for many ML functions by passing a flag to the `apply` method. The supported functions include: (1) **Atomic ML Functions** such as `matMul`, `matAdd`, `conv`, `softmax`, `argmax`, `pooling`, `relu`, `batchNormalization`, `cosSim` (cosine similarity), `concat`, `dropout`, `embed` (embedding lookup), `decisionTree`, `standard/min/maxScalarization`, `seqEncode` (i.e., encoding a sequence of tokens into an embedding vector), and `binarization`; (2) **High-level ML Functions** such as feed-forward neural network model (`ffnn`), convolutional neural network (`cnn`), decision forest model (`xgboost/lightgbm`), Huggingface inference endpoints (`huggingface`), and ChatGPT APIs (`llm`). These functions take one or more vectors/tensor objects as input, e.g., $W_i \in \mathbf{W}$, $vec \in \mathbf{V}, vec \in block$ as described in Sec. III-A.

Importantly, a user can register customized atomic and high-level functions in addition to these built-in ML functions.

C. IR Overview

To maximize co-optimization opportunities by enabling each sub-computation to select its optimal computation and data abstraction, we propose a novel three-level IR:

Top-level IR: Relational Algebra. In the top-level IR, every node is a relational operator, which is customized by an expression opaque at this level. Each edge represents a data flow from the source node to the destination node.

Middle-level IR: Expression Tree. An opaque expression from the top-level IR is lowered to the middle-level IR as an expression tree, where each node is either an expression operator (see Sec. III-B) or an opaque sub-expression.

Bottom-level IR: ML Computation Graph. An opaque sub-expression in the middle-level IR is lowered to the bottom-level IR as a computation graph that is understandable to the query optimizer. In the bottom-level IR, each node represents an atomic ML function (see Sec. III-B), while each edge represents a tensor output from the source node and input to the destination node. From the bottom-level IR, each atomic ML function’s details, such as input tensor shapes, the shapes of model weight matrices, etc., can be retrieved by the query optimizer from the ML function instance through pre-defined interfaces.

Our IR design allows a query optimizer to rewrite more than one level of IRs at the same time to support any co-optimization techniques from O1-O4 in arbitrary ordering for any sub-computation, maximizing co-optimization space, as shown in the next section.

D. Workflow: from a Query to Our IR

As illustrated in Fig. 3, at Step 1, a user loads a two-tower recommendation model, which is a popular type of recommendation models [25], [65]. In our example, the

model consists of a user tower and a movie tower. The two towers encode user features and movie features into vectors, respectively. The cosine similarity between the user vector and the movie vector is then computed to decide whether the movie should be recommended to the user. During the model loading process [66], all ML functions required by the model are developed if needed (can build on existing AI/ML libraries), customized, registered, and used to compose a computational graph. At Step 2, the computational graph is registered as the `twoTowerModel` expression. At Step 3, a query is issued that applies the `twoTowerModel` expression to compute a recommendation score for each pair of preprocessed user and movie features. At Step 4, the query is translated into a three-level IR, where the top `project3` node in the top-level IR points to a middle-level IR that only contains the opaque `twoTowerModel` expression, which links to the detailed bottom-level IR registered at Step 3.

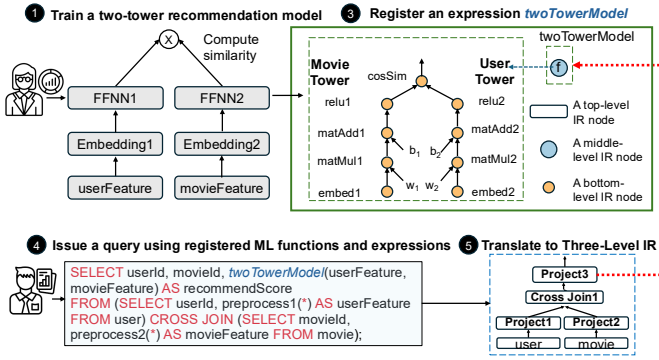


Fig. 3: Develop and Translate an Inference Query to Our IR.

E. Examples of Using Our IR

Fig. 4 presents three transformations of the 3-level IR from our running example in Fig. 3.

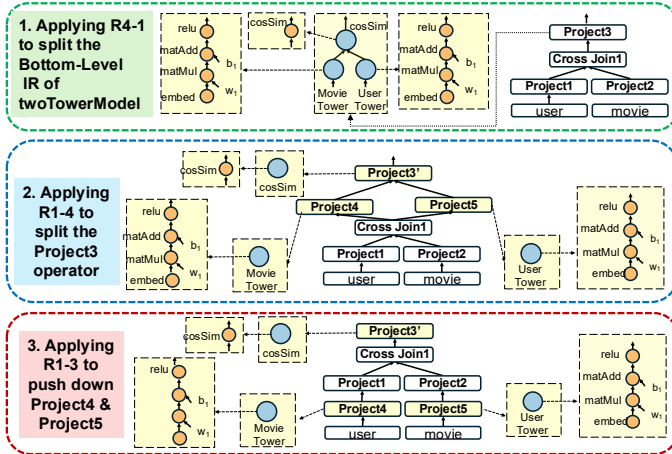


Fig. 4: Example Transformations of our three-level IR.

As shown in Fig. 4-1, the optimizer first splits the `twoTowerModel` expression into three parts: the user tower, the movie tower, and an operator that computes their cosine similarity (See R4-1 in Sec. II-A). In Fig. 4-2, the node `Project3` in the top-level IR is split into `Project3'`

corresponding to cosine similarity, `Project4` corresponding to movie tower, and `Project5` corresponding to user tower (See R1-4 in Sec. II-A). Then, in Fig. 4-3, `Project4` and `Project5` are pushed down to avoid redundant computations (See R1-3 in Sec. II-A).

IV. QUERY OPTIMIZATION

In this section, we will describe our unique query optimization process co-designed with our three-level IR representation. The goal is to address the search space challenge via a novel reusable MCTS model based on query embedding techniques.

A. MCTS Preliminary

MCTS has become a popular tool for query optimization [43], [46]. That is because MCTS can efficiently explore a large search space, e.g., various rewrite ordering, by balancing exploration and exploitation, guaranteeing asymptotic convergence to the optimal decision once combined node selection strategies such as UCB [67]. A common abstraction of MCTS for query optimization includes the following components:

States, i.e., a node in the MCTS tree, represents a logical query plan of the SQL query to be optimized and the input datasets. **Node Utility Function**. Every state is associated with a utility representing the cumulative reward of the state and indicating the probability that the state is in the optimal path.

Actions. Usually, an action, i.e., an edge in the MCTS tree, refers to a rewriting or equivalent transformation of the current plan, transitioning it to a new plan that produces equivalent results. The applicable rewriting and transformation rules defines the action space.

Runtime Search Process. The MCTS algorithm starts with the root node, the initial query plan. At each step, it checks whether the current state has been expanded, i.e., all rewriting rules of the given state have been explored. If so, the MCTS selects an action based on UCB (Line 1 of Alg. 1), where r_i is the utility of $node_i$ (the accumulative reward of $node_i$), n_i is the number of total visits of the $node_i$, N_i is the total number of visits of the parent node of $node_i$, and c is a constant for balancing exploration ($\frac{r_i}{n_i}$) and exploitation ($c \cdot \sqrt{\frac{\ln N_i}{n_i}}$). If the current node is not fully expanded, it will expand the node by randomly selecting one unexplored action (see Alg. 2). Then, it performs a simulation, also called a rollout, as described in Alg. 3. The rollout process randomly chooses an action until it reaches a maximum number of iterations or the terminating state (i.e., no more applicable rules). After rolling out, it will run a back-propagation process to compute rewards and update the utility of each selected node, described in Alg. 4. See supplementary material for the overall algorithm.

Algorithm 1: $select(node)$

Input: $node$: the current state of the given query
1 $selectedNode \leftarrow \underset{node_i \in node.children}{\operatorname{argmax}} \frac{r_i}{n_i} + c \cdot \sqrt{\frac{\ln N_i}{n_i}}$;
2 **return** $selectedNode$;

Shortcomings of the naive MCTS optimization. As a runtime query planner, MCTS constructs a search tree from scratch for every query, making optimization inefficient. In addition,

Algorithm 2: *expand(node)*

Input: *node*: the current state of the given query
1 *unexplored* $\leftarrow \{a \in \text{node.actionSpace} \mid a.\text{explored} == \text{False}\}$;
2 *selectedAction* $\leftarrow \text{randomSelect}(\text{unexplored})$;
3 *selectedAction.explored* $\leftarrow \text{True}$;
4 *node'* $\leftarrow \text{node.takeAction}(\text{selectedAction})$;
5 *node.children* $\leftarrow \text{node.children} \cup \{\text{node}'\}$;
6 **return** *node'* ;

Algorithm 3: *rollout(node)*

Input: *node*: the node where simulation starts
1 **while** *node.isTerminateState()* $== \text{False}$ **do**
2 *selectedAction* $\leftarrow \text{RandomSelect}(\text{node.actionSpace})$;
3 *node* $\leftarrow \text{node.takeAction}(\text{selectedAction})$;
4 **return** *node* ;

simply caching MCTS states for reuse cannot fully resolve the problem, because in practice, repeated queries often use different parameters [68], which have unique states and action spaces, preventing tree reuse even among similar queries.

Therefore, the naive MCTS model cannot exploit such similarity to reduce query optimization latency.

B. Reusable MCTS based on Query Embedding

Recent Query2Vec techniques encode SQL queries into fixed-length vectors for downstream tasks such as query optimization (e.g., BAO [69], NEO [70]), cost estimation (e.g., E2E-Cost [71], RTOS [72]), and join/index selection (e.g., ReJOIN [73], AIMeetsAI [74]). More recently, QueryFormer [75] leverages transformers for general-purpose embeddings. We build on this line of work by encoding logical query plans into embedding vectors to enable MCTS to generalize across queries and improve optimization efficiency. However, existing methods are faced with the following challenges.

Challenge-1. *Existing query2vec models did not consider inference queries in three-level IR forms, and they cannot capture expressions and ML functions.*

Challenge-2. *While the query embedding can be used to unify the state space for different queries, the action space remains query-specific. It is difficult to integrate Query2Vec with MCTS to navigate the full co-optimization space.*

To address the challenges, we offer a novel reusable MCTS framework co-designed with our three-level IR, by extending QueryFormer [75], the state-of-the-art query embedding technique that is capable of capturing the structural information of the query plan [76].

1) *Embedding the Three-level IR:* QueryFormer [75], like other query embedding methods, is designed for tree-based query plans rather than query plans represented in our three-level IR. This is done by encoding each node’s attributes, such as *operator type*, *join type*, *input table*, *filter predicate*, *histograms of the related columns*, and *bitmap of samples* into embedding vectors E_o , E_j , E_t , E_p , E_h , and E_s respectively. These vectors are concatenated to form a fixed-length node vector. Each node vector is further added with a height encoding vector that specifies the node’s position in the query graph. The query graph is then abstracted as a sequence of node vectors

Algorithm 4: *backpropagate(node, reward)*

Input: *node*: the node where simulation starts; *reward*: the reward value obtained from reward function
1 **while** *node* $\neq \text{NULL}$ **do**
2 $n_i \leftarrow n_i + 1$;
3 $r_i \leftarrow r_i + \text{reward}$;
4 *node* $\leftarrow \text{node.parent}$;
5 **return** ;

following the in-order tree traversal. The sequence is sent to a transformer model, which outputs the final embedding vector for the entire query tree.

To address **Challenge-1**, we adopt a recursive encoding strategy that captures the rich hierarchical structure of the three-level IR. At the bottom level, each opaque expression is encoded into an embedding vector E_{expr} (see Step 1 of Fig. 5). These are then composed into middle-level IR embeddings, which are used to encode corresponding relational operators. Finally, the top-level IR, comprising these embedded relational operators, is processed by a QueryFormer-like model to generate the final query embedding (see Step 2 of Fig. 5).

Embedding of Bottom-Level IR. We employ a QueryFormer-like, transformer-based Model2Vec to embed a bottom-level IR into a vector representation in the following approach: (1) For each opaque expression at a middle-level IR, a **breadth-first traversal** is applied to its corresponding bottom-level IR (if present), to encode each node (e.g., an ML function) into a vector by concatenating the following components:

- E_{mlType} : Encodes the ML function type, preserving function diversity. It is generated through an embedding layer, where the parameters are learned during the training process.
- $E_{mlFlops}$: Captures the computational cost of the node as the number of floating point operations (FLOPs).
- E_{mlDims} : Records the shape of the tensor dimensions.

The resulting bottom-level IR graph, where each node is represented as a feature vector, is then passed to the Model2Vec to generate the final embedding vector, E_{expr} , for the expression.

Embedding of an Entire Query. Similar to QueryFormer, for each relational operator in the top-level IR, we first extract feature vectors for E_o , E_j , E_t , E_p , E_h , and E_s . Here, if the operator’s middle-level IR contains an opaque expression that maps to a bottom-level IR encoded as E_{expr} , E_i is constructed similarly to QueryFormer [75] except that it sees the bottom-level IR’s output as an output column encoded by E_{expr} . Then, each feature vector E_i is scaled to a fixed size through a linear layer. The resulting vectors are then concatenated to construct the top-level node embedding vector:

$$V = \parallel \text{LinearLayer}_i(E_i), i \in \{o, j, t, p, h, s, expr\} \quad (1)$$

where \parallel is the concatenation. We then map the query plan into a sequence of m vectors (V_1, \dots, V_m) corresponding to m top-level IR nodes following in-order tree traversal of the top-level IR, which is sent to a QueryFormer-like Query2Vec model [75] to output a final embedding vector for the query plan represented in our three-level IR. This design enables the estimation of selectivity via two complementary mechanisms.



Fig. 5: CACTUSDB's Query Optimization Workflow.

First, for native SQL filters, selectivity features are explicitly encoded via the histogram and filter predicate embeddings. Second, for AI/ML filters, selectivity is learned implicitly by combining the model embedding with the table and column embeddings. During the training process, the model learns the latent relationships between the model's input and output distribution, capturing the predicate's selectivity.

While the architectures of our Model2Vec and Query2Vec models are similar to QueryFormer [75], we redesign the loss function for two tasks: (1) query embedding for matching a query to an MCTS state; and (2) execution latency prediction for MCTS reward computation. We train these two tasks separately, because joint training of both objectives resulted in gradient interference, degrading the cost estimation accuracy. Decoupling these tasks outperforms the single-model strategy as discussed in Sec. V-E.

Task 1. Query Embedding for MCTS State Matching. We combine contrastive learning with Weisfeiler-Lehman (WL) kernel, a widely used and effective method for capturing structural similarity of graphs [77], to map semantically similar expressions and query plans closer in the Model2Vec and Query2Vec embedding spaces while pushing dissimilar ones apart [78], [79]. The corresponding contrastive loss is defined in Eq. 2, where N is the number of training samples, \mathbf{z}_i denotes the embedding vector of the anchor sample, \mathbf{z}_i^+ and \mathbf{z}_i^- are its positive and negative examples, $\text{sim}(\mathbf{z}_1, \mathbf{z}_2)$ denotes cosine similarity $\frac{\mathbf{z}_1^\top \mathbf{z}_2}{\|\mathbf{z}_1\| \cdot \|\mathbf{z}_2\|}$, and τ is a temperature hyperparameter.

$$\text{Loss}_{\text{contrastive}} = \frac{1}{N} \sum_{i=1}^N \mathcal{L}_i \quad (2)$$

$$\mathcal{L}_i = -\log \frac{\exp(\text{sim}(\mathbf{z}_i, \mathbf{z}_i^+)/\tau)}{\exp(\text{sim}(\mathbf{z}_i, \mathbf{z}_i^-)/\tau) + \exp(\text{sim}(\mathbf{z}_i, \mathbf{z}_i^+)/\tau)} \quad (3)$$

To train our Model2Vec and Query2Vec models via contrastive learning, we construct positive and negative pairs using structural similarity quantified by the WL subtree kernel [80]. In each WL iteration, node labels are updated by hashing the current label with the multiset of neighbor labels, capturing rich local structures. Each graph is represented by a feature vector of normalized label frequencies, and similarity is computed via cosine similarity. In Model2Vec, node labels are initialized by ML function type and FLOPs in the bottom-level IR. Functions of the same type share the same label only if their FLOPs differ within a threshold. In Query2Vec, the initial label for each relational operator encodes operator type, input table, columns, and the WL features of associated expressions. Although WL features define contrastive pairs, they cannot replace embedding models at runtime, as unseen queries may yield varying label counts and inconsistent feature lengths.

Task 2. Latency Prediction for Cost Estimation. We leverage the Query2Vec embeddings to predict the query execution

latency, which is used by calculating the reward. This prediction is implemented via a four-layer FFNN that takes the query embedding as input and predicts the estimated latency. The loss function defined in Eq. 4, is based on mean squared error (MSE), where \hat{y}_i and y_i denote the predicted latency and ground-truth latency of the i -th sample, respectively.

$$\text{Loss}_{\text{latency}} = \frac{1}{N} \sum_{i=1}^N (y_i - \hat{y}_i)^2 \quad (4)$$

We adopt a two-model design. Query2Vec is first trained via contrastive learning for embedding generation, and a separate copy is retrained with an FFNN for latency prediction.

2) *Reusable MCTS with Configurable Actions:* To address the **Challenge-2**, we proposed a unique MCTS abstraction:

Embedding-based States. We use our recursive embedding strategy described in the previous sections to convert each logical query plan into a 393-dimensional embedding vector to represent a state. (This dimensionality is determined by Eq. 1. Following QueryFormer [75], each of E_o , E_j , E_t , E_h , and E_s is 64-dimensional, The predicate E_p consists of the filter embedding (64-dimensional), operator embedding (8-dimensional), and a normalized scalar value (1-dimensional).)

Configurable Actions. Each action corresponds to a high-level co-optimization rule (Sec. II), making the action space universal across queries. When a rule is selected via UCB, we configure the rule to decide how to apply it to the query. For example, if R3-1 is selected, we must choose a `matMul` function to convert to relational operators. We first use heuristics, if available, to narrow the candidates, e.g., we select the `matMul` functions involving the top- k largest tensors. We then identify the optimal candidate that maximizes cost reduction under R3-1 using our embedding-based latency predictor as the cost estimator. The configured rule is then applied to transition the current state to the next state, transforming the query plan. This approach allows for a universal action space, addressing Challenge-2.

Runtime Search. A subtree of an MCTS tree may be shared by query plans with similar embedding vectors. As illustrated in Alg. 5, in the online planning process, a query's default plan will be converted into an embedding vector using our Query2Vec model, denoted as M_{Q2V} . As illustrated in Step 3 of Fig. 5, it then performs a nearest neighbor search across the nodes in existing MCTS trees. If there is no matching state with which the cosine similarity is smaller than a threshold, a new MCTS tree needs to be constructed from scratch. Otherwise, it will resume the MCTS search process starting from the matched state, as shown in Step 4 of Fig. 5. Note that in the highlighted sequence of transformation rules that are selected by MCTS, we have R4-1, followed by R2-1, and R1-3, as explained in Sec. III-E.

Reward. Upon reaching a terminate state, T , MCTS computes the reward as the overall cost reduction, as the overall cost

Algorithm 5: Search with Reusable MCTS

Input: *query*: a query applied with simple predicate push-down and join reordering; M_{Q2V} : a model embedding *query* to a vector; $B_iteration$: the maximum number of iterations; *mctsTreeSet*: A set of existing MCTS trees; *nodeIndex*: An index of embedding vectors of existing MCTS tree nodes.

```
/* Convert the query into an embedding vector */
1 queryEmbed ←  $M_{Q2V}(query)$  ;
/* Find nearest neighbor in the MCTS trees */
2 if nodeIndex.count(queryEmbed) then
3   /* Start training from the searched node */
4   root ← nodeIndex.getNearestNeighbor(queryEmbed);
5 else
6   /* Otherwise, initialize a new MCTS tree */
7   root ← TreeNode(queryEmbed) ;
8   mctsTreeSet.add(root);
9 for i in range(B_iteration) do
10  node ← root ;
11  while node.isTerminateState() == False do
12    if node.expanded then
13      node ← select(node) ;
14    else
15      node ← expand(node) ;  $T \leftarrow rollout(node)$  ;
16      break;
17  reward ← computeReward(T) ;
18  backpropagate(node, reward);
/* After search, update node indexes */
19 nodeIndex.update(node);
20 return;
```

reduction of the plan, i.e., $reward = cost_{root} - cost_T$. This reward is then backpropagated following Alg. 4, while the remaining search process follows the general MCTS procedure described in Sec. IV-A.

3) *Error Bound Analysis*: We model CactusDB’s reusable MCTS-based query optimization as search in a depth- d expectimax tree [81] rooted at the initial logical plan s_0 . Let \mathcal{S} denote ground states (logical plans), \mathcal{A} rewrite actions, and \mathcal{T} the set of ground trajectories up to depth d . The optimal action-value and value functions over trajectories are defined as follows, where $\mathcal{P}(t, a, t')$ represents that the transition probability of t to t' (one step extension of t) for $a \in \mathcal{A}$. We also have $\mathcal{R}(t)$ denoting the reward of selecting trajectory $t \in \mathcal{T}$.

$$Q^*(t, a) = \mathcal{R}(t) + \sum_{t'} \mathcal{P}(t, a, t') V^*(t'), \quad (5)$$

$$V^*(t) = \max_{a \in \mathcal{A}} Q^*(t, a). \quad (6)$$

CactusDB applies a query embedding function $f : \mathcal{S} \rightarrow \mathcal{X}$ to aggregate ground states into abstract states, inducing a partition of trajectories into abstract histories \mathcal{H} . Reusable MCTS shares statistics among trajectories within each abstract history, effectively optimizing over the resulting abstract expectimax tree. Following prior analysis of MCTS with state aggregation [81], we assume the embedding f satisfies (p, q) -consistency: for every abstract history $h \in \mathcal{H}$, there exists an action that is uniformly p -near-optimal for all ground trajectories in h , and the optimal values of any two trajectories in h differ by at most q . Under this assumption, the abstraction-induced error accumulates linearly with search depth.

Theorem 1 (Reusable MCTS error bound under (p, q) -consistency). *Let $a^\#$ be the action selected at the root by optimizing over the abstract MCTS tree. Then the suboptimality of $a^\#$ in the ground MDP is bounded by*

$$\left| \max_{a \in \mathcal{A}} Q^*(s_0, a) - Q^*(s_0, a^\#) \right| \leq 2d(p + q).$$

The full analysis with formal proof is provided in Appendix D and E.

Empirical Error Bound We additionally derived an empirical error bound using Latin Hypercube Sampling (LHS) to systematically cover the query embedding space. Specifically, we sampled 200 queries (from queries in Sec. V-C5), and for each query, used our reusable MCTS framework to optimize it with the optimized execution latency t . We then performed exhaustive search to obtain the ground-truth optimal latency t^* . Across all sampled queries, we observed a mean relative error of 0.9661% with a standard deviation of 0.6355%. The corresponding 95% confidence interval ranges from 0.8771% to 1.0551%. Here, the relative error is defined as $\frac{(t-t^*)}{t}$, which is assumed to follow a normal distribution, as is common practice [82].

V. EXPERIMENTAL EVALUATION

In this section, we present our implementation and compare the end-to-end inference query latency of CACTUSDB with baseline systems, followed by an ablation study on the benefits of integrating co-optimization rules. We also evaluate the effectiveness and overheads of our query optimization strategy.

A. Implementation

We implemented our three-level IR and our reusable MCTS query optimizer using Velox [47] as a backend. We leveraged Velox’s query parser and expression parser to support the top-level and middle-level IR, while implementing all ML functions to support the bottom-level IR on our own. The action space of our query optimizer includes all co-optimization rules as discussed in Sec. II-A. Our optimizer is applied after rule-based join reordering is executed and before Velox’s physical query optimization (e.g., filter reordering and adaptive column prefetching [47]) is performed. All existing MCTS tree nodes are stored in Faiss [83], a well-known vector database, with cosine similarity indexing to accelerate nearest neighbor search.

To generate training data for Model2Vec, we defined a set of model templates—including two-tower recommendation models, Deep Learning Recommendation Model (DLRM) [84], autoencoders, singular value decomposition (SVD) [85], convolutional neural networks, FFNN, embedding models, decision forests, and others (details are provided in Appendix M). From these templates, we randomly sampled 10,000 ML models of varying hyperparameters (e.g., number of neurons, number of layers, number of trees, tree depth, etc.) to construct the training data, with 80% for training and 20% for testing. The trained Model2Vec model is used for embedding the ML expressions to build the feature vectors for the Query2Vec model as described in Sec. IV-B1. The downstream model inference latency prediction task achieves an average Q-Error [75], [86]

of 1.1 and a Pearson correlation of 98.02%, demonstrating its effectiveness in capturing the complexity of ML models. (Q-Error, defined as $Q(c) = \max(\frac{actual(c)}{predicted(c)}, \frac{predicted(c)}{actual(c)})$, is widely used for cost estimation [75], [86].)

To train the Query2Vec model, we generated 10,000 training queries using 14 out of 20 query templates described in Sec. V-C5. We further split them into 80% training and 20% testing sets to evaluate the model’s performance. Our two-model strategy achieved a median Q-Error of 1.19 and 94% correlation between predicted and actual latency, outperforming the one-model strategy, which achieved a median Q-Error of 1.6 and 90% correlation. It is important to note that for query optimization, preserving the relative ranking of query plans is more critical than absolute prediction accuracy. The high correlation confirms that our model effectively preserves the relative ranking of candidate query plans. This allows MCTS to reliably explore the search space.

B. Baselines

We compared the end-to-end query processing latency of CACTUSDB to the following baselines: **EvaDB** (v0.3.9), which uses Postgres as backend, provides an AI-centric query optimizer focusing on result caching, query predicate reordering, and parallel query processing [10], [53]. **Apache PySpark w/ UDF** (v3.5.0), which allows model inferences via UDFs [87], [88], with data stored in HDFS. **MADLib** (v2.1.0), which extends Postgres with ML functions [24]. **SystemDS** (v3.2.0), provides a declarative language for data science and ML pipelines, built on Apache Spark [56], [89]. **PostgresML** (v2.10.0), a Postgres extension for ML [11]. **IMBridge**, accelerates in-DB ML inference by caching model contexts and batching predictions efficiently. **DL-Centric**, where data is stored in Postgres database (v14.15), and then data is transferred into PyTorch (v2.1.2) using ConnectorX (v0.3.2) [90] for model inferences. Its end-to-end query latency includes both in-database processing time, data transfer time, and model inference time.

We also compared the end-to-end latency and the query optimization latency of our reusable MCTS query optimizer with the following optimization algorithms, all applied after join-reordering and before Velox physical query optimization. **Un-optimized**. The query runs without co-optimization.

Arbitrary Co-optimization. It scans all co-optimization rules and applies all applicable rules [43].

Heuristics-based. (1) it will aggressively push down the `filter/ project` operators; (2) it will aggressively fuse ML operators; (3) Tensor relational transformations are applied only if the model size exceeds a threshold (half of the available memory size).

Vanilla MCTS. It builds an MCTS search tree following the naive MCTS search process as described in Sec. IV-A. Both our proposed MCTS optimizer and vanilla optimizer use the learned cost estimation model based on query embeddings, described in Sec. IV-B1.

Reusable. We evaluated two versions of our reusable MCTS optimizer with the embedding and cost estimation models trained

using the one-model and two-model strategies respectively, as described in Sec. IV-B1 and Sec. V-A.

Evaluation Environment. Most experiments were conducted on an AWS r4.2xlarge instance (8 CPU cores, 61 GB memory). The query optimizer evaluation ran on an Ubuntu machine (48 CPU cores, 125 GB memory). GPU experiments used an AWS g4dn.4xlarge instance (16 CPU cores, one T4 GPU with 16 GB memory and 64 GB host memory).

C. Benchmarks

We used five benchmarks, reflecting realistic industrial query scenarios. These benchmarks nest more than ten diverse AI/ML model architectures with complex SQL queries. Most queries involve up to ten ML functions, 1-4 `join/crossJoin` operators, 2-5 filters, 1-7 projection operators, and up to 4 `aggregate/groupBy` operators, ensuring a comprehensive evaluation of co-optimization strategies. See Appendix I, J, and N for detailed queries.

1) *Recommendation Queries*.: The MovieLens dataset [48], [49] is widely used for evaluating DB-for-ML works [49], [56], [91]–[93]. We used MovieLens-1M dataset, which collected 1 million ratings from 6,000 users for 4,000 movies and augmented it with movie tag relevance data from MovieLens-32M dataset, which provides 140,979 unique tags and per-movie relevance vectors. We developed three realistic recommendation queries based on existing studies. Q1 is derived from [65] for pre-ranking systems. It aggregates user and movie features from ratings, applies an FFNN model and a “LIKE” filter to select trending movies within a given movie genre, and cross-joins them with users for scoring via a widely used industrial pre-ranking model, two-tower model [94]. Q2 and Q3 are adopted from real-world production pipelines described in the multi-stage recommendation technical blog [95] for building intelligent recommender systems. Q2 applies a movie trending FFNN and a user-interest FFNN to prefilter user-movie pairs, then joins them with movie relevance tag table where an AutoEncoder [96] is used to transform the high-dimensional movie-tag vector into a low-dimensional dense representation. The output is passed to a DLRM [84] to estimate a recommendation score. Q3 uses two FFNN-based filters to identify movies that users may be interested in. For each user-movie pair, a vector similarity search is performed using cosine similarity on the movie’s dense representation obtained via the AutoEncoder.

2) *Retailing-Complex Queries*.: To evaluate performance on complex, modern model architectures not currently covered by existing benchmarks, we designed three realistic inference queries for trip classification (Q1), credit card fraud detection (Q2), and product recommendation (Q3) using the TPCx-AI dataset [50] with scale-factors 1 and 10. While maintaining the original schema relations, we replaced the simpler default models with production-grade deep learning architectures, including FFNN, XGBoost, and Two-Tower models. Q1 joins the *Order* and *Store* tables, applies an ML filter to remove unqualified orders and purchases, and sends the results to an FFNN model for trip classification. Q2 aggregates the *Order*

table to generate per-customer features, which is joined with the *Transaction* table and the *Customer* table. The resulting features are sent to an *XGBoost* model and an FFNN model, and return transactions identified as fraud by *both* models. Q3 first filters and aggregates the *product_rating*. The output is joined with the *product* table to embed text attributes as product vectors. Similar processing is applied to the *customer* table to obtain the customer features. The two are cross-joined and sent to a two-tower model that ranks *product-customer* pairs.

3) *Retailing-Simplified Queries*: We found baselines such as MADLib, SystemDS, and PostgresML do not natively support first two benchmarks involving complex AI/ML functions and multiple AI/ML filters. For fair comparisons, we evaluated three simplified queries directly adopted from the official TPCx-AI benchmark with scale-factors 1 and 10 for product rating, trip classification, and fraud detection. Q1 applies an SVD model [85] to factorize the *product_rating* matrix for product recommendation. Q2 uses a 50-tree XGBoost model to classify trips based on aggregated features joined from the *store* and *order* tables. Q3 applies logistic regression for fraud detection by joining the features from *financial_account* and *financial_transaction* tables.

4) *Other Analytics Queries*: We also evaluated three analytics workloads on real-world datasets - fraud detection on the Credit Card dataset [51] (Q1), hotel ranking prediction on Expedia dataset [52] (Q2), and codeshare classification on Flights dataset [52] (Q3), which are widely used for evaluating in-DB ML systems [38], [64]. At initial scale (Scale=1), the ML inputs have around 289,000 rows and 29 features for Q1, 79,000 rows and 3,000 features for Q2, and 7,000 rows and 6,000 features for Q3. We further evaluate them at Scale=10, which increases the row count by 10 \times . The Credit Card workload performs a single table scan. Expedia performs a three-way join across *listings*, *hotel*, and *search* tables. Flights performs a four-way join across *routes*, *airlines*, *source*, and *destination airports*. All the workloads apply 4-6 predicate filters, then standardizes numerical and one-hot-encodes categorical columns. The resulting features feed into tree-based classifiers - a single decision tree for Expedia and a 100-tree ensemble (max depth 9) for Credit Card and Flights. Additionally, we include the state-of-the-art IMBridge [64], [97], as a baseline, which focuses on UDF-level optimization for inference queries. It is excluded from the previous benchmark due to its limited support for complex models used in that settings.

5) *A Large-Scale Randomly Generated Inference Query Benchmark*: We designed 20 inference query templates including 10 for the MovieLens dataset, and 10 for TPCx-AI dataset (Scale-1). To eliminate selection bias, we derived these templates from community and industry standards. For MovieLens, we crawled the most highly-voted data science notebooks from Kaggle [98] and abstracted their logic. These templates cover recommendation, rating prediction, collaborative filtering, and rating analysis, using two-tower recommendation models, DLRM, AutoEncoders, SVD, and FFNN. For TPCx-AI, we adopted the queries from its official use cases, including

recommendation, trip classification, fraud and spam detection, customer segmentation, and sales prediction, employing decision forests, SVD, FFNN, logistic regression, and K-Means. Additional details are available in our Appendix M and N. Each sampled query varies in model architecture (e.g., different number of layers and neurons for FFNN models), numbers and selectivity of filter predicates. Following [76], we divide the query templates into two groups: six randomly chosen from both workloads form the out-of-distribution set used solely for evaluation, while the remaining 14 generate both training and evaluation queries under different random seeds. We generated 10,000 queries for training the query embedding and cost estimation models, and an additional 1,000 in-distribution and 1,000 out-of-distribution queries to evaluate our optimizer’s generalization capability.

D. Overall Performance Comparison

TABLE I: End-to-End Latency Comparison of Complex Queries

		O1	O2	O3	O4	Latency	
Recommendation Queries	Q1	CACTUSDB	✓		✓	0.15 sec	
		EvaDB	✓			42.80 sec	
		Apache PySpark w/ UDF	✓			60.28 sec	
		DL-Centric			✓	48.88 sec	
	Q2	CACTUSDB	✓	✓	✓	✓	3.35 sec
		EvaDB	✓				Failed (OOM)
		Apache PySpark w/ UDF	✓				Failed (OOM)
		DL-Centric				✓	142.96 sec
	Q3	CACTUSDB	✓		✓	✓	6.62 sec
		EvaDB	✓				Failed (OOM)
		Apache PySpark w/ UDF	✓				Failed (OOM)
		DL-Centric				✓	207.12 sec
Retailing-Complex Queries	Q1	CACTUSDB	✓	✓		72.07 sec	
		EvaDB	✓			123.24 sec	
		Apache PySpark w/ UDF	✓			307.88 sec	
		DL-Centric				✓	163.97 sec
	Q2	CACTUSDB	✓		✓	✓	44.38 sec
		EvaDB	✓				275.76 sec
		Apache PySpark w/ UDF	✓				1320.47 sec
		DL-Centric				✓	304.81 sec
	Q3	CACTUSDB	✓			✓	3.46 sec
		EvaDB	✓				119.62 sec
		Apache PySpark w/ UDF	✓				1525.94 sec
		DL-Centric				✓	403.84 sec

Complex Inference Queries. As shown in Tab. I, CACTUSDB significantly outperformed the other systems across all six complex queries. CACTUSDB achieved 22 – 401 \times speedup on recommendation queries, and 1.7 – 441 \times speedup on retailing queries, in terms of end-to-end latency compared to the fastest baseline.

We further analyzed the optimization cost, ranging from 0.02s to 0.35s. The specific overhead ratios for the six queries are 13%, 3.8%, 3.7%, 0.5%, 0.7%, and 0.8%, respectively. Notably, across the entire workload, the optimization phase accounts for only approximately 1% of the total cumulative execution time. We further conducted a detailed analysis of the optimizer performance in Sec. V-E.

Beyond latency, we profiled the peak memory usage to evaluate resource efficiency (Fig. 6). CACTUSDB demonstrated superior memory management, peaking at only 14% usage even for heavy workloads. In contrast, baselines suffered from higher memory usage, which can lead to OOM errors when the model is too large. CACTUSDB avoids memory bottlenecks through our query optimizer, which actively selects plans that minimize intermediate data volumes.

(1) Recommendation queries. For Q1, CACTUSDB factorized the two-tower model (R4-1, R1-4) and pushed down the user tower and movie tower through the *cross-join* (R1-3), leading to a significant reduction in overall latency. For

Q1, EvaDB achieved the second-best performance. However, it needs to transfer the data from the database to the Python runtime for inferences, which accounted for 16% of the end-to-end time. For Q2 and Q3, CACTUSDB transforms the `matMul` in a large AutoEncoder model (that encodes the high-dimensional sparse tag matrix into a low-dimensional dense representation) to relational processing (R3-1). This optimization greatly reduced memory footprint. In contrast, EvaDB and the UDF-based PySpark implementation struggled with handling large matrix computations, resulting in out-of-memory (OOM) errors. DL-Centric implementation suffers from cross-system feature transfer overhead, which accounts for 37% of end-to-end time.

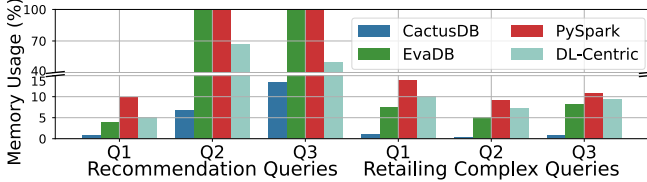


Fig. 6: Memory Usage Comparison for Complex Inference Queries

(2) Retailing-Complex queries. CACTUSDB significantly outperforms all baselines across the three queries, achieving the highest speedup on Q3 (product recommendation). The gain is mainly driven by splitting user-product feature computations (R4-1) and pushdown (R1-3). For trip type classification (Q1) and fraudulent transaction detection (Q2), performance gain stems from factorizing `matMul` (R2-1) and the transformation of XGBoost to `crossJoin` and `aggregate` (R3-2), respectively. Additional improvements come from reordering and pushing down AI/ML filters (R1-1 and R1-2). In contrast, EvaDB and DL-Centric incur high latency from database-Python transfer and costly operators, such as matrix multiplication and XGBoost, while UDF-based PySpark performs worst due to missing UDF optimizations.

Retailing-Simplified Queries. Fig. 7 shows that CACTUSDB consistently achieved the best performance across all three queries at both scale factors, yielding 1.7–20.8× speedups over the fastest baseline. MADLib outperforms well for Q1 and Q2 at scale factor 1, but it internally relies on Python runtime (e.g., scikit-learn’s SVD and XGBoost) introduces extra overhead. In Q2 with scale factor 10, MADLib introduces additional recursive function calls during XGBoost inference as the data size increases, leading to significant performance degradation. In Q3, its native logistic regression is less efficient than scikit-learn’s highly optimized implementation. For PostgresML, its batch prediction API is significantly faster than its regular prediction API but implemented as an aggregation operator, preventing simultaneous access to non-group-by attributes and causing inefficiency in Q2. It also lacks SVD model support for Q1. SystemDS exhibits slower inference due to less optimized XGBoost and SVD implementations, while DL-Centric suffers from data transfer overhead despite leveraging high-performance ConnectorX library [90].

Other Analytics Queries. As shown in Fig. 8, CACTUSDB outperforms the best of other baselines by 2 – 2.5× at scale-

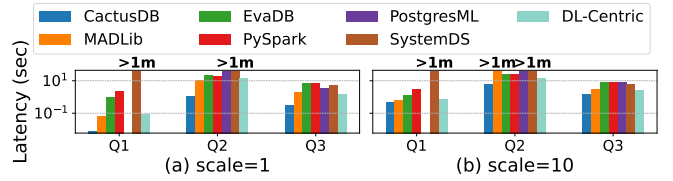


Fig. 7: Latency Comparison for Retailing-Simplified Queries (Log Scale). ">1m" indicates latency greater than 1 minute.

1 and 1.2 – 5.7× at scale-10. PostgresML is slightly slower (1.5× and 1.2× slower) than CACTUSDB on the first two queries on scale-10 data, but struggles with the larger Q3 workload that contains many rows, on which it is 66× slower than CACTUSDB. IMBridge benefits from batch processing and context caching but suffers from data transfer overhead between the database query engine and the model inference backend when data size increased. Although Pyspark and SystemDS benefit from their parallel execution and exhibit more stable runtimes, CACTUSDB outperformed PySpark by 1.6 – 9.2× and SystemDS by 1.6 – 9.5× on scale-10 data. EvaDB and MADLib underperform other baselines for these workloads.

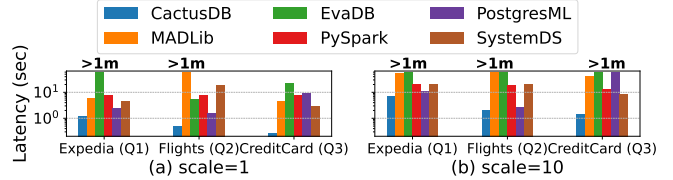


Fig. 8: Latency Comparison for Three Analytics Queries (Log Scale). ">1m" indicates latency greater than 1 minute.

Ablation Study. To understand the benefits of integrating all co-optimization rules, we compare the performance of applying all optimization techniques versus only one category on the recommendation and retailing-complex queries. As shown in Tab. II, integrating all co-optimization rules yields substantially higher speedups than using only one category. For example, Recommendation-Q1 achieves 676.1× speedup over the default plan by pushing down filters and factorizing model computation to avoid redundant inference.

TABLE II: Ablation Study

Workloads	Queries	Un-optimized	O1	O2	O3	O4	Combined
Recommendation	Q1	1.0X	45.1X	NA	NA	10.9X	676.1X
	Q2	1.0X	3.8X	2.9X	1.8X	2.0X	18.5X
	Q3	1.0X	3.5X	NA	2.1X	1.5X	12.4X
Retailing	Q1	1.0X	1.3X	1.5X	NA	1.2X	1.9X
	Q2	1.0X	1.7X	2.0X	1.5X	1.6X	4.3X
	Q3	1.0X	2.9X	15.8X	NA	2.6X	28.3X

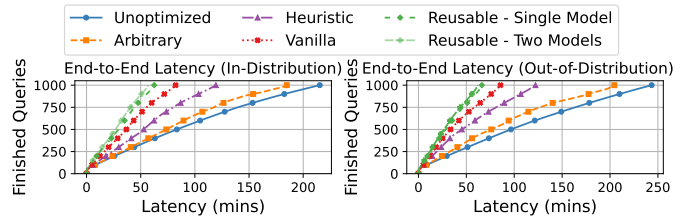


Fig. 9: Query Optimizer Comparison on End-to-End Latency

E. Evaluation of Reusable MCTS Optimizer

In this section, we compare our reusable MCTS inference query optimizer with alternative optimization strategies in

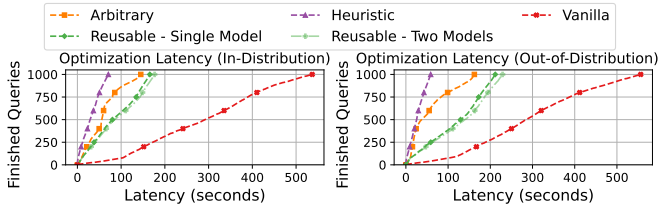


Fig. 10: Query Optimizer Comparison on Optimization Latency

terms of end-to-end latency and optimization overhead on 1,000 in-distribution (ID) queries and 1,000 out-of-distribution (OOD) queries. Results are reported as elapsed latency versus the number of finished queries in Fig. 9 and Fig. 10. The results revealed that the reusable MCTS effectively balances optimization overheads and execution latency by reusing MCTS search trees across queries.

For ID queries, the reusable MCTS achieves an 89% state collision rate (i.e., the ratio of queries matching existing MCTS states) greatly reducing optimization time compared to vanilla MCTS. While, vanilla MCTS produces high-quality query plans, it incurs substantial optimization overhead due to the need of rebuilding a search tree from scratch for each query, becoming a bottleneck as shown in Fig. 10. The heuristic optimizer performs better than the arbitrary baseline but often produces suboptimal plans due to its fixed rule order.

Our reusable MCTS also generalizes well to OOD queries. Initially, OOD queries require building new MCTS trees due to the absence of reusable states, resulting in higher optimization latency, but optimization efficiency improves as more reusable states are found. On average, the state collision rate reaches 72%, indicating strong generalization. As shown in Fig. 9 and Fig. 10, our two-model strategy introduces minor optimization overhead —6% for ID and 7% for OOD queries. However, the improved query plan latency estimation leads to better optimization results, achieving 10% and 7% improvements in end-to-end execution latency, respectively.

Storage Overhead Analysis The Model2Vec and Query2Vec models occupy 8MB and 23MB, respectively. We incrementally maintain MCTS search trees, where each node requiring about 1.6KB of storage. Thanks to MCTS tree reusability, the overall storage cost remains low. For instance, optimizing 1,000 queries requires less than 2MB in total.

VI. RELATED WORK

Prior in-database AI/ML systems and unified intermediate representations (IRs) support only subsets of SQL-ML co-optimization techniques (O1-O4). UDF-centric systems such as EvaDB [10], PostgresML [11], MADLib [24], and PySpark [99] primarily enable O1-style relational rewrites while treating AI/ML logic as opaque, which precludes deeper co-optimization. Factorized ML systems [26]–[29], [54], [100] support O2-style optimization for predefined models or linear algebra operators, but focus mainly on training and lack integration with general inference pipelines. Other systems and IRs, including SimSQL [31], [55], SystemML/SystemDS [56], [89], MASQ [41], [101], Raven [38], SDQL [60], Weld [36],

[37], Lara [59], LingoDB [102], [103], and Tensor Relational Algebra [30], combine relational, linear algebra, and ML operators to varying degrees, yet none of them support flexible decomposition of inference pipelines with end-to-end optimization across O1-O4.

Existing inference optimizers rely largely on rule-based, cost-based, or learned strategies (e.g., Spark Catalyst [104], [105], Cascades-style CBOs [106]–[108], and learned optimizers [9], [43], [69], [109]), which struggle with arbitrary AI/ML workloads and ad-hoc inference queries. In contrast, CACTUSDB is a unified in-database inference system that supports relational, linear-algebra, and ML operators within a three-level IR, decomposes inference pipelines into fine-grained sub-computations, and employs a learning-assisted optimizer to efficiently explore a large co-optimization search space, enabling systematic composition of O1-O4 techniques.

VII. CONCLUSION

In this paper, we present CACTUSDB, a system that enables efficient execution and automatic optimization of SQL-ML queries. CACTUSDB is the first database system that supports applying diverse co-optimization techniques to different sub-computations of one inference query by introducing a flexible and expressive three-level IR. To efficiently explore the enlarged search space resulting from the integration of co-optimization techniques, we propose a novel, reusable MCTS-based optimizer co-designed with our three-level IR. Unlike existing MCTS-based query optimizers, ours represents query plans as embedding vectors (states) and co-optimization techniques as configurable actions, enabling MCTS state sharing across queries. CACTUSDB achieved $1.7\times$ to $441\times$ speedup over the fastest baseline systems across 11 inference workloads. Evaluation on 2,000 inference queries further demonstrates that our reusable MCTS optimizer achieved better effectiveness-efficiency trade-offs than alternative optimizers.

Limitations and Future Works First, CACTUSDB currently lacks a user-friendly front-end for converting existing Python-based data science pipelines into our three-level IR forms. As a result, integrating legacy workflows requires manual effort and a learning curve. Second, similar to Raven [38], the CACTUSDB query optimizer relies on a predefined set of machine learning functions and rewrite rules to support various co-optimization techniques. Introducing new co-optimization strategies that involve novel AI/ML functions requires additional engineering effort to implement the corresponding functions and explicitly inform the optimizer of the associated rewrite actions. Third, the current implementation represents complex models, such as large language models (LLMs), as black boxes, due to the challenge of converting these models to compact computational graphs. Consequently, CACTUSDB can only apply a subset of co-optimization techniques to these models.

Future work includes (1) developing user-friendly toolchains to facilitate the import of legacy code and the extension of the query optimizer to new ML functions and rewrite rules, and (2) representing LLMs as white-box models to enable more effective co-optimization techniques.

VIII. AI-GENERATED CONTENT ACKNOWLEDGEMENT

No generative AI tools were used to generate the content in this submission, including text, figures, tables, and code.

IX. ACKNOWLEDGMENTS

We sincerely thank Saif Masood and Qi Lin for their contributions to the development of ML functions and rewrite actions at an early stage of this project. We also thank the anonymous reviewers from VLDB'25, SIGMOD'26, and ICDE'26 for their constructive and insightful feedback. This work was supported by the National Science Foundation (NSF) CAREER Award (No. 2144923) and an Amazon Research Award.

REFERENCES

- [1] C. Ruan, A. Stewart, H. Li, R. Ye, D. Vengerov, and H. Wang, "Dynamic embedding-based retrieval for personalized item recommendations at instacart," in *Companion Proceedings of the ACM Web Conference 2023*, 2023, pp. 983–987.
- [2] L. Patel, S. Jha, C. Guestrin, and M. Zaharia, "Lotus: Enabling semantic queries with llms over tables of unstructured and structured data," *arXiv preprint arXiv:2407.11418*, 2024.
- [3] C. Liu, M. Russo, M. Cafarella, L. Cao, P. B. Chen, Z. Chen, M. Franklin, T. Kraska, S. Madden, and G. V. Itagliano, "A declarative system for optimizing ai workloads," *arXiv preprint arXiv:2405.14696*, 2024.
- [4] N. Katkov, "Operationalizing fraud prevention on ibm z16," 2022. [Online]. Available: <https://www.ibm.com/downloads/cas/DOXY3Q94>
- [5] T. Kraska, A. Beutel, E. H. Chi, J. Dean, and N. Polyzotis, "The case for learned index structures," in *Proceedings of the 2018 International Conference on Management of Data*, 2018, pp. 489–504.
- [6] A. Sharma, X. Li, H. Guan, G. Sun, L. Zhang, L. Wang, K. Wu, L. Cao, E. Zhu, A. Sim *et al.*, "Automatic data transformation using large language model-an experimental study on building energy data," in *2023 IEEE International Conference on Big Data (BigData)*. IEEE, 2023, pp. 1824–1834.
- [7] L. Zhou, K. S. Candan, and J. Zou, "Deepmapping: Learned data mapping for lossless compression and efficient lookup," in *2024 IEEE 40th International Conference on Data Engineering (ICDE)*. IEEE, 2024, pp. 1–14.
- [8] H. Guan, Y. Wang, L. Xie, S. Nag, R. Goel, N. E. N. Swamy, Y. Yang, C. Xiao, J. Prisby, R. Maciejewski *et al.*, "Idnet: A novel dataset for identity document analysis and fraud detection," *arXiv preprint arXiv:2408.01690*, 2024.
- [9] G. Li, J. Sun, L. Xu, S. Li, J. Wang, and W. Nie, "Gaussml: An end-to-end in-database machine learning system," in *2024 IEEE 40th International Conference on Data Engineering (ICDE)*, 2024, pp. 5198–5210.
- [10] G. T. Kakkar, J. Cao, P. Chunduri, Z. Xu, S. R. Vyalla, P. Dintyala, A. Prabhakaran, J. Bang, A. Sengupta, K. Ravichandran *et al.*, "Eva: An end-to-end exploratory video analytics system," in *Proceedings of the Seventh Workshop on Data Management for End-to-End Machine Learning*, 2023, pp. 1–5.
- [11] "postgresml," <https://postgresml.org/docs/introduction/getting-started>, 2024.
- [12] L. Zhou, Q. Lin, K. Chowdhury, S. Masood, A. Eichenberger, H. Min, A. Sim, J. Wang, Y. Wang, K. Wu *et al.*, "Serving deep learning models from relational databases," *Advances in Database Technology-EDBT*, vol. 27, no. 3, pp. 717–724, 2024.
- [13] Q. Lin, S. Wu, J. Zhao, J. Dai, M. Shi, G. Chen, and F. Li, "Smartlite: A dbms-based serving system for dnn inference in resource-constrained environments," *Proceedings of the VLDB Endowment*, vol. 17, no. 3, pp. 278–291, 2023.
- [14] H. Shahrokhi, A. Kholi, M. Ghorbani, and A. Shaikhha, "Pytond: Efficient python data science on the shoulders of databases," in *2024 IEEE 40th International Conference on Data Engineering (ICDE)*. IEEE, 2024, pp. 423–435.
- [15] A. Shaikhha, M. Schleich, and D. Olteanu, "An intermediate representation for hybrid database and machine learning workloads," *Proceedings of the VLDB Endowment*, vol. 14, no. 14 (12), pp. 2831–2834, 2021.
- [16] K. Chowdhury, L. Zhou, L. Xie, X. Fu, and J. Zou, "Inferf: Declarative factorization of ai/ml inferences over joins," *arXiv preprint arXiv:2511.20489*, 2025.
- [17] H. Guan, A. Tiwari, S. Gautier, R. H. Ambrish, L. Zhou, Y. Wang, D. Gupta, Y. Yang, C. Xiao, K. Chowdhury *et al.*, "Declarative privacy-preserving inference queries," in *International Conference on Database Systems for Advanced Applications*. Springer, 2025, pp. 502–506.
- [18] K. Chowdhury, L. Xie, L. Zhou *et al.*, "Exboost: Out-of-box co-optimization of machine learning and join queries," 2025.
- [19] B. Yuan, D. Jankov, J. Zou, Y. Tang, D. Bourgeois, and C. Jermaine, "Tensor relational algebra for machine learning system design," *arXiv preprint arXiv:2009.00524*, 2020.
- [20] H. Guan, S. Masood, M. Dwarampudi, V. Gunda, H. Min, L. Yu, S. Nag, and J. Zou, "A comparison of end-to-end decision forest inference pipelines," in *Proceedings of the 2023 ACM Symposium on Cloud Computing*, 2023, pp. 200–215.
- [21] G. J. Annas, "Hipaa regulations: a new era of medical-record privacy?" *New England Journal of Medicine*, vol. 348, p. 1486, 2003.
- [22] "The total cost of ownership (tco) of amazon sagemaker," 2022, accessed: 2024-12-20. [Online]. Available: <https://pages.awscloud.com/NAMER-In-GC-400-machine-learning-sagemaker-tco-learn-ty.html>
- [23] D. Crankshaw, "The design and implementation of low-latency prediction serving systems," Ph.D. dissertation, UC Berkeley, 2019.
- [24] J. M. Hellerstein, C. Ré, F. Schoppmann, D. Z. Wang, E. Fratkin, A. Gorajek, K. S. Ng, C. Welton, X. Feng, K. Li *et al.*, "The madlib analytics library," *Proceedings of the VLDB Endowment*, vol. 5, no. 12, 2012.
- [25] J. Yang, X. Yi, D. Zhiyuan Cheng, L. Hong, Y. Li, S. Xiaoming Wang, T. Xu, and E. H. Chi, "Mixed negative sampling for learning two-tower neural networks in recommendations," in *Companion proceedings of the web conference 2020*, 2020, pp. 441–447.
- [26] M. Schleich, D. Olteanu, and R. Ciucanu, "Learning linear regression models over factorized joins," in *Proceedings of the 2016 International Conference on Management of Data*, 2016, pp. 3–18.
- [27] L. Chen, A. Kumar, J. Naughton, and J. M. Patel, "Towards linear algebra over normalized data," *Proc. VLDB Endow.*, vol. 10, no. 11, p. 1214–1225, Aug. 2017. [Online]. Available: <https://doi.org/10.14778/3137628.3137633>
- [28] S. Li, L. Chen, and A. Kumar, "Enabling and optimizing non-linear feature interactions in factorized linear algebra," in *Proceedings of the 2019 International Conference on Management of Data*, 2019, pp. 1571–1588.
- [29] M. Schleich, D. Olteanu, M. Abo Khamis, H. Q. Ngo, and X. Nguyen, "A layered aggregate engine for analytics workloads," in *Proceedings of the 2019 International Conference on Management of Data*, ser. SIGMOD '19. New York, NY, USA: Association for Computing Machinery, 2019, p. 1642–1659. [Online]. Available: <https://doi.org/10.1145/3299869.3324961>
- [30] B. Yuan, D. Jankov, J. Zou, Y. Tang, D. Bourgeois, and C. Jermaine, "Tensor relational algebra for distributed machine learning system design," *Proc. VLDB Endow.*, vol. 14, no. 8, pp. 1338–1350, 2021. [Online]. Available: <http://www.vldb.org/pvldb/vol14/p1338-yuan.pdf>
- [31] D. Jankov, S. Luo, B. Yuan, Z. Cai, J. Zou, C. Jermaine, and Z. J. Gao, "Declarative recursive computation on an rdbms," *Proceedings of the VLDB Endowment*, vol. 12, no. 7, 2019.
- [32] J. Zou, R. M. Barnett, T. Lorido-Bofran, S. Luo, C. Monroy, S. Sikdar, K. Teymourian, B. Yuan, and C. Jermaine, "Plinycompute: A platform for high-performance, distributed, data-intensive tool development," in *Proceedings of the 2018 International Conference on Management of Data*, 2018, pp. 1189–1204.
- [33] J. Zou, A. Das, P. Barhate, A. Iyengar, B. Yuan, D. Jankov, and C. Jermaine, "Lachesis: automatic partitioning for udf-centric analytics," *Proceedings of the VLDB Endowment*, vol. 14, no. 8, pp. 1262–1275, 2021.
- [34] J. Zou, A. Iyengar, and C. Jermaine, "Pangea: monolithic distributed storage for data analytics," *Proceedings of the VLDB Endowment*, vol. 12, no. 6, pp. 681–694, 2019.
- [35] —, "Architecture of a distributed storage that combines file system, memory and computation in a single layer," *The VLDB Journal*, pp. 1–25, 2020.
- [36] S. Palkar, J. J. Thomas, A. Shanbhag, D. Narayanan, H. Pirk, M. Schwarzkopf, S. Amarasinghe, M. Zaharia, and S. InfoLab, "Weld: A common runtime for high performance data analytics," in *Conference on Innovative Data Systems Research (CIDR)*, 2017, p. 45.

- [37] S. Palkar, J. Thomas, D. Narayanan, P. Thaker, R. Palamuttam, P. Negi, A. Shanbhag, M. Schwarzkopf, H. Pirk, S. Amarasinghe *et al.*, “Evaluating end-to-end optimization for data analytics applications in weld,” *Proceedings of the VLDB Endowment*, vol. 11, no. 9, pp. 1002–1015, 2018.
- [38] K. Park, K. Saur, D. Banda, R. Sen, M. Interlandi, and K. Karanasos, “End-to-end optimization of machine learning prediction queries,” in *Proceedings of the 2022 International Conference on Management of Data*, 2022, pp. 587–601.
- [39] M. Schleich, A. Shaikhha, and D. Suci, “Optimizing tensor programs on flexible storage,” *Proceedings of the ACM on Management of Data*, vol. 1, no. 1, pp. 1–27, 2023.
- [40] X. Meng, J. Bradley, B. Yavuz, E. Sparks, S. Venkataraman, D. Liu, J. Freeman, D. Tsai, M. Amde, S. Owen *et al.*, “Mllib: Machine learning in apache spark,” *The Journal of Machine Learning Research*, vol. 17, no. 1, pp. 1235–1241, 2016.
- [41] F. Del Buono, M. Paganelli, P. Sottovia, M. Interlandi, and F. Guerra, “Transforming ml predictive pipelines into sql with masq,” in *Proceedings of the 2021 International Conference on Management of Data*, 2021, pp. 2696–2700.
- [42] C. B. Browne, E. Powley, D. Whitehouse, S. M. Lucas, P. I. Cowling, P. Rohlfshagen, S. Tavener, D. Perez, S. Samothrakis, and S. Colton, “A survey of monte carlo tree search methods,” *IEEE Transactions on Computational Intelligence and AI in games*, vol. 4, no. 1, pp. 1–43, 2012.
- [43] X. Zhou, G. Li, C. Chai, and J. Feng, “A learned query rewrite system using monte carlo tree search,” *Proceedings of the VLDB Endowment*, vol. 15, no. 1, pp. 46–58, 2021.
- [44] X. Yu, C. Chai, G. Li, and J. Liu, “Cost-based or learning-based? a hybrid query optimizer for query plan selection,” *Proceedings of the VLDB Endowment*, vol. 15, no. 13, pp. 3924–3936, 2022.
- [45] Q. Bai, S. Alsudais, C. Li, and S. Zhao, “Maliva: Using machine learning to rewrite visualization queries under time constraints,” in *EDBT*, 2023, pp. 157–170.
- [46] S. Sikdar and C. Jermaine, “Monsoon: Multi-step optimization and execution of queries with partially obscured predicates,” in *Proceedings of the 2020 ACM SIGMOD International Conference on Management of Data*, 2020, pp. 225–240.
- [47] P. Pedreira, O. Erling, M. Basmanova, K. Wilfong, L. Sakka, K. Pai, W. He, and B. Chattopadhyay, “Velox: meta’s unified execution engine,” *Proceedings of the VLDB Endowment*, vol. 15, no. 12, pp. 3372–3384, 2022.
- [48] F. M. Harper and J. A. Konstan, “The movielens datasets: History and context,” *Acm transactions on interactive intelligent systems (tiis)*, vol. 5, no. 4, pp. 1–19, 2015.
- [49] M. Sarwat, R. Moraffah, M. F. Mokbel, and J. L. Avery, “Database system support for personalized recommendation applications,” in *2017 IEEE 33rd International Conference on Data Engineering (ICDE)*. IEEE, 2017, pp. 1320–1331.
- [50] C. Brücke, P. Härtling, R. D. E. Palacios, H. Patel, and T. Rabl, “Tpcx-ai—an industry standard benchmark for artificial intelligence and machine learning systems,” *Proceedings of the VLDB Endowment*, vol. 16, no. 12, pp. 3649–3661, 2023.
- [51] “Kaggle credit card fraud dataset,” 2013, accessed: 2025-07-15. [Online]. Available: <https://www.kaggle.com/mlg-ulb/creditcardfraud>
- [52] Project Hamlet, “Project hamlet,” <https://adalabucsd.github.io/hamlet.html>, 2021, accessed: 2025-07-15.
- [53] G. T. D. Group, “Evadb optimization,” <https://evadb.readthedocs.io/en/stable/source/reference/optimizations.html>, 2023, accessed: 2025-01-03.
- [54] Z. Huang, R. Sen, J. Liu, and E. Wu, “Joinboost: Grow trees over normalized data using only sql,” *Proc. VLDB Endow.*, vol. 16, no. 11, p. 3071–3084, Jul. 2023. [Online]. Available: <https://doi.org/10.14778/3611479.3611509>
- [55] S. Luo, Z. J. Gao, M. Gubanov, L. L. Perez, and C. Jermaine, “Scalable linear algebra on a relational database system,” *ACM SIGMOD Record*, vol. 47, no. 1, pp. 24–31, 2018.
- [56] M. Boehm, M. W. Dusenberry, D. Eriksson, A. V. Evfimievski, F. M. Manshadi, N. Pansare, B. Reinwald, F. R. Reiss, P. Sen, A. C. Surve *et al.*, “Systemml: Declarative machine learning on spark,” *Proceedings of the VLDB Endowment*, vol. 9, no. 13, pp. 1425–1436, 2016.
- [57] L. Zhou, J. Chen, A. Das, H. Min, L. Yu, M. Zhao, and J. Zou, “Serving deep learning models with deduplication from relational databases,” *Proc. VLDB Endow.*, vol. 15, no. pp. 2230–2243, 2022. [Online]. Available: <https://www.vldb.org/pvldb/vol15/p2230-zou.pdf>
- [58] J. Zou, M. Zhao, J. Shi, and C. Wang, “Watson: A workflow-based data storage optimizer for analytics,” in *Proceedings of the 36th International Conference on Massive Storage Systems and Technology (MSST 2020)*.
- [59] A. Kunft, A. Katsifodimos, S. Schelter, S. Breß, T. Rabl, and V. Markl, “An intermediate representation for optimizing machine learning pipelines,” *Proceedings of the VLDB Endowment*, vol. 12, no. 11, pp. 1553–1567, 2019.
- [60] A. Shaikhha, M. Huot, J. Smith, and D. Olteanu, “Functional collection programming with semi-ring dictionaries,” *Proceedings of the ACM on Programming Languages*, vol. 6, no. OOPSLA1, pp. 1–33, 2022.
- [61] A. Vasudevan, A. Anderson, and D. Gregg, “Parallel multi channel convolution using general matrix multiplication,” in *2017 IEEE 28th international conference on application-specific systems, architectures and processors (ASAP)*. IEEE, 2017, pp. 19–24.
- [62] “Implementation of convolution as matrix multiplication.” [Online]. Available: <https://cs231n.github.io/convolutional-networks/>
- [63] “Optimizing tensorflow convolution performance on aarch64,” 2016, archived at <https://web.archive.org/web/20211127091024/https://www.linaro.org/blog/optimizing-tensorflow-convolution-performance-on-aarch64>.
- [64] C. Zhang, J. Peng, C. Xu, Q. Xu, and C. Yang, “Imbridge: Impedance mismatch mitigation between database engine and prediction query execution,” in *Companion of the 2024 International Conference on Management of Data*, 2024, pp. 456–459.
- [65] X. Li, B. Chen, H. Guo, J. Li, C. Zhu, X. Long, S. Li, Y. Wang, W. Guo, L. Mao *et al.*, “Inttower: the next generation of two-tower model for pre-ranking system,” in *Proceedings of the 31st ACM International Conference on Information & Knowledge Management*, 2022, pp. 3292–3301.
- [66] “Cactusdb’s model loading example,” <https://anonymous.4open.science/r/CactusDB/velox/optimizer/tests/ModelLoadingTest.cpp>, 2026.
- [67] H. S. Chang, M. C. Fu, J. Hu, and S. I. Marcus, “An adaptive sampling algorithm for solving markov decision processes,” *Operations Research*, vol. 53, no. 1, pp. 126–139, 2005.
- [68] Z. Wu, R. Marcus, Z. Liu, P. Negi, V. Nathan, P. Pfeil, G. Saxena, M. Rahman, B. Narayanaswamy, and T. Kraska, “Stage: Query execution time prediction in amazon redshift,” in *Companion of the 2024 International Conference on Management of Data*, 2024, pp. 280–294.
- [69] R. Marcus, P. Negi, H. Mao, N. Tatbul, M. Alizadeh, and T. Kraska, “Bao: Making learned query optimization practical,” in *Proceedings of the 2021 International Conference on Management of Data*, 2021, pp. 1275–1288.
- [70] R. Marcus, P. Negi, H. Mao, C. Zhang, M. Alizadeh, T. Kraska, O. Papaemmanouil, and N. Tatbul, “Neo: A learned query optimizer,” *arXiv preprint arXiv:1904.03711*, 2019.
- [71] J. Sun and G. Li, “An end-to-end learning-based cost estimator,” *arXiv preprint arXiv:1906.02560*, 2019.
- [72] X. Yu, G. Li, C. Chai, and N. Tang, “Reinforcement learning with tree- lstm for join order selection,” in *2020 IEEE 36th international conference on data engineering (ICDE)*. IEEE, 2020, pp. 1297–1308.
- [73] R. Marcus and O. Papaemmanouil, “Deep reinforcement learning for join order enumeration,” in *Proceedings of the First International Workshop on Exploiting Artificial Intelligence Techniques for Data Management*, 2018, pp. 1–4.
- [74] B. Ding, S. Das, R. Marcus, W. Wu, S. Chaudhuri, and V. R. Narasayya, “Ai meets ai: Leveraging query executions to improve index recommendations,” in *Proceedings of the 2019 International Conference on Management of Data*, 2019, pp. 1241–1258.
- [75] Y. Zhao, G. Cong, J. Shi, and C. Miao, “Queryformer: A tree transformer model for query plan representation,” *Proceedings of the VLDB Endowment*, vol. 15, no. 8, pp. 1658–1670, 2022.
- [76] Y. Zhao, Z. Li, and G. Cong, “A comparative study and component analysis of query plan representation techniques in ml4db studies,” *Proceedings of the VLDB Endowment*, vol. 17, no. 4, pp. 823–835, 2023.
- [77] Z. Cai, X. Li, B. Hui, M. Yang, B. Li, B. Li, Z. Cao, W. Li, F. Huang, L. Si *et al.*, “Star: Sql guided pre-training for context-dependent text-to-sql parsing,” *arXiv preprint arXiv:2210.11888*, 2022.
- [78] T. Gao, X. Yao, and D. Chen, “Simcse: Simple contrastive learning of sentence embeddings,” *arXiv preprint arXiv:2104.08821*, 2021.
- [79] S. Chen, J. Fan, B. Wu, N. Tang, C. Deng, P. Wang, Y. Li, J. Tan, F. Li, J. Zhou *et al.*, “Automatic database configuration debugging using retrieval-augmented language models,” *Proceedings of the ACM on Management of Data*, vol. 3, no. 1, pp. 1–27, 2025.

- [80] N. Shervashidze, P. Schweitzer, E. J. Van Leeuwen, K. Mehlhorn, and K. M. Borgwardt, "Weisfeiler-lehman graph kernels." *Journal of Machine Learning Research*, vol. 12, no. 9, 2011.
- [81] J. Hostetler, A. Fern, and T. Dietterich, "State aggregation in monte carlo tree search," in *Proceedings of the AAAI Conference on Artificial Intelligence*, vol. 28, no. 1, 2014.
- [82] C. Chang, E. Lo, and C. Ye, "Biathlon: Harnessing model resilience for accelerating ml inference pipelines," *Proceedings of the VLDB Endowment*, vol. 17, no. 10, pp. 2631–2640, 2024.
- [83] J. Johnson, M. Douze, and H. Jégou, "Billion-scale similarity search with GPUs," *IEEE Transactions on Big Data*, vol. 7, no. 3, pp. 535–547, 2019.
- [84] M. Naumov, D. Mudigere, H.-J. M. Shi, J. Huang, N. Sundaraman, J. Park, X. Wang, U. Gupta, C.-J. Wu, A. G. Azzolini *et al.*, "Deep learning recommendation model for personalization and recommendation systems," *arXiv preprint arXiv:1906.00091*, 2019.
- [85] M. E. Wall, A. Rechtsteiner, and L. M. Rocha, "Singular value decomposition and principal component analysis," in *A practical approach to microarray data analysis*. Springer, 2003, pp. 91–109.
- [86] T. Siddiqui, A. Jindal, S. Qiao, H. Patel, and W. Le, "Cost models for big data query processing: Learning, retrofitting, and our findings," in *Proceedings of the 2020 ACM SIGMOD International Conference on Management of Data*, 2020, pp. 99–113.
- [87] A. Spark, "Pyspark," <https://spark.apache.org/docs/latest/api/python/index.html>, 2024, accessed: 2025-01-03.
- [88] Databricks, "Model inference using pytorch," <https://docs.databricks.com/en/machine-learning/model-inference/resnet-model-inference-pytorch.html>, 2023, accessed: 2025-01-03.
- [89] M. Boehm, I. Antonov, S. Baunsgaard, M. Dokter, R. Ginhör, K. Innerebner, F. Klezin, S. Lindstaedt, A. Phani, B. Rath *et al.*, "Systemds: A declarative machine learning system for the end-to-end data science lifecycle," *arXiv preprint arXiv:1909.02976*, 2019.
- [90] X. Wang, W. Wu, J. Wu, Y. Chen, N. Zrymiak, C. Qu, L. Flokas, G. Chow, J. Wang, T. Wang *et al.*, "Connectox: accelerating data loading from databases to dataframes," *Proceedings of the VLDB Endowment*, vol. 15, no. 11, pp. 2994–3003, 2022.
- [91] S. Wooders, X. Mo, A. Narang, K. Lin, I. Stoica, J. M. Hellerstein, N. Crooks, and J. E. Gonzalez, "Ralf: Accuracy-aware scheduling for feature store maintenance," *Proceedings of the VLDB Endowment*, vol. 17, no. 3, pp. 563–576, 2023.
- [92] C. Qin, M. Torres, and F. Rusu, "Scalable asynchronous gradient descent optimization for out-of-core models," *Proceedings of the VLDB Endowment*, vol. 10, no. 10, pp. 986–997, 2017.
- [93] M. Ghorbani and A. Shaikhha, "Demonstration of opendbml, a framework for democratizing in-database machine learning," *Proceedings of the VLDB Endowment*, vol. 16, no. 12, pp. 3970–3973, 2023.
- [94] P.-S. Huang, X. He, J. Gao, L. Deng, A. Acero, and L. Heck, "Learning deep structured semantic models for web search using clickthrough data," in *Proceedings of the 22nd ACM international conference on Information & Knowledge Management*, 2013, pp. 2333–2338.
- [95] (2024) Deploying a multi-stage recommender system. NVIDIA Merlin. Accessed: 2026-01-08. [Online]. Available: <https://nvidia-merlin.github.io/Merlin/stable/examples/Building-and-deploying-multi-stage-RecSys/index.html>
- [96] G. E. Hinton and R. R. Salakhutdinov, "Reducing the dimensionality of data with neural networks," *science*, vol. 313, no. 5786, pp. 504–507, 2006.
- [97] C. Zhang, J. Peng, C. Xu, Q. Xu, and C. Yang, "Mitigating the impedance mismatch between prediction query execution and database engine," *Proc. ACM Manag. Data*, vol. 3, no. 3, Jun. 2025. [Online]. Available: <https://doi.org/10.1145/3725326>
- [98] S. Claudia, "Movielens dataset," <https://www.kaggle.com/datasets/sherinclaudia/movielens>, 2019, accessed: 2025-05-17.
- [99] P. Singh and P. Singh, "Manage data with pyspark," *Machine Learning with PySpark: With Natural Language Processing and Recommender Systems*, pp. 15–37, 2022.
- [100] A. Kumar, J. Naughton, and J. M. Patel, "Learning generalized linear models over normalized data," in *Proceedings of the 2015 ACM SIGMOD International Conference on Management of Data*, ser. SIGMOD '15. New York, NY, USA: Association for Computing Machinery, 2015, p. 1969–1984. [Online]. Available: <https://doi.org/10.1145/2723372.2723713>
- [101] M. Paganelli, P. Sottovia, K. Park, M. Interlandi, and F. Guerra, "Pushing ml predictions into dbmss," *IEEE Transactions on Knowledge and Data Engineering*, vol. 35, no. 10, pp. 10 295–10 308, 2023.
- [102] M. Jungmair, A. Kohn, and J. Giceva, "Designing an open framework for query optimization and compilation," *Proceedings of the VLDB Endowment*, vol. 15, no. 11, pp. 2389–2401, 2022.
- [103] M. Jungmair and J. Giceva, "Declarative sub-operators for universal data processing," *Proceedings of the VLDB Endowment*, vol. 16, no. 11, pp. 3461–3474, 2023.
- [104] H. Pirahesh, J. M. Hellerstein, and W. Hasan, "Extensible/rule based query rewrite optimization in starburst," *ACM Sigmod Record*, vol. 21, no. 2, pp. 39–48, 1992.
- [105] M. Armbrust, R. S. Xin, C. Lian, Y. Huai, D. Liu, J. K. Bradley, X. Meng, T. Kaftan, M. J. Franklin, A. Ghodsi *et al.*, "Spark sql: Relational data processing in spark," in *Proceedings of the 2015 ACM SIGMOD International Conference on Management of Data*. ACM, 2015, pp. 1383–1394.
- [106] G. Graefe, "The cascades framework for query optimization," *IEEE Data Eng. Bull.*, vol. 18, no. 3, pp. 19–29, 1995.
- [107] Apache Software Foundation, *Apache Calcite: Dynamic Data Management Framework*, 2024, accessed February 2025. [Online]. Available: <https://calcite.apache.org/>
- [108] The PostgreSQL Global Development Group, "Postgresql," 2025, accessed February 2025. [Online]. Available: <https://www.postgresql.org/>
- [109] R. Marcus, P. Negi, H. Mao, C. Zhang, M. Alizadeh, T. Kraska, O. Papaemmanouil, and N. Tatbul, "Neo: a learned query optimizer," *Proceedings of the VLDB Endowment*, vol. 12, no. 11, pp. 1705–1718, 2019.
- [110] C. Lucchese, F. M. Nardini, S. Orlando, R. Perego, N. Tonello, and R. Venturini, "Quickscore: A fast algorithm to rank documents with additive ensembles of regression trees," in *Proceedings of the 38th International ACM SIGIR Conference on Research and Development in Information Retrieval*, 2015, pp. 73–82.
- [111] —, "Quickscore: Efficient traversal of large ensembles of decision trees," in *Joint European Conference on Machine Learning and Knowledge Discovery in Databases*. Springer, 2017, pp. 383–387.
- [112] T. P. Foundation, *LibTorch: PyTorch C++ API*, 2018. [Online]. Available: <https://pytorch.org/cppdocs/>
- [113] T. White, *Hadoop: The Definitive Guide*. O'Reilly Media, 2012.
- [114] M. Zaharia, M. Chowdhury, M. J. Franklin, S. Shenker, and I. Stoica, "Spark: cluster computing with working sets," in *USENIX HotCloud*, 2010, pp. 1–10.
- [115] C. Lattner, M. Amini, U. Bondhugula, A. Cohen, A. Davis, J. Pienaar, R. Riddle, T. Shpeisman, N. Vasilache, and O. Zinenko, "Mlir: A compiler infrastructure for the end of moore's law," *arXiv preprint arXiv:2002.11054*, 2020.
- [116] "Tpcx-ai express benchmark," 2021. [Online]. Available: <https://www.tpc.org/tpcx-ai/default5.asp>

A. An Extensive List of SQL-ML Co-Optimization Techniques

We summarize (non-approximate) SQL-ML co-optimization techniques into four main categories, O1-O4. We also highlight the disparate data abstraction (focusing on model parameter representation) and computation abstraction across these categories.

O1. Nested Relational Algebra Optimization [9], [11], [24], [53]. The computation abstraction consists of relational operators such as `filter`, `project`, `join`, `crossJoin`, and `aggregate`. Each operator can be customized by an expression consisting of expression operators, such as `=`, `>`, `<`, `^`, `CALLFUNC` (i.e., invoking an arbitrary opaque function for feature processing, AI/ML model inferences, etc.). In the data abstraction, each weight tensor used by the AI/ML models is encapsulated in the functions, opaque to the query optimizer. Example co-optimization techniques in O1 include:

(Notations: A and B are two attributes of the table R , of vector type and float type respectively, and k is a constant.)

R1-1 filter Reorder. It reorders two `filters` that are customized by user-defined expressions such as $dnnFraudDetect(R.A) = True$ and $R.B > k$, so that the one with smaller selectivity is executed first to reduce the amount of data input to the other.

R1-2 filter Expression Merge and Factorization. Two `filters` with different boolean expressions on the same dataset, can be merged into one filter with combined expressions in which redundant computations can be removed, e.g., $f(R.A) = True \wedge R.B > k$ and $R.B < k - 1$ (a naive example) can be merged into $false$. Factorization is the reverse process of merging.

R1-3 filter Pushdown/Pullup. A `filter` can be pushed down through a `join` to avoid redundant evaluation of the `filter`'s expression over repeated records caused by the `join`, if the `join`'s output has a high cardinality. Otherwise, the `filter` should be pulled up to avoid evaluating expressions over records that do not have a match through the `join`.

R1-4 project Merge and Factorization. Similar to R1-2, two consecutive `projects` customized by expressions can be merged into one `project` with optimized expressions. Factorization is the reverse process of merging.

R1-5 project Pushdown/Pullup. Similar to R1-3, `project` with expressions can be pushed down/pulled up to avoid redundant/unnecessary computations.

O2. Factorized Inference (derived from factorized ML [27]–[29]). The computation abstraction consists of relational operators and a limited set of factorizable ML functions, such as inner product of vector and weight matrix. For data abstraction, parameters of a factorizable ML function are stored as a factorizable object, visible to the query optimizer. Example co-optimization techniques include:

(Notations: $S(Y, X_S, FK)$ and $R(RID, X_R)$ are two tables. X_S and X_R are the feature vectors. RID is the key attribute of R , and FK is a foreign key of S referencing RID . Y is the union of rest columns in S . After joining S and R on $FK = RID$, we can obtain an output table $T(Y, X)$, where $X \equiv [X_S, X_R]$ is the concatenation of the feature vectors.)

R2-1 Linear Algebra Operator Factorization [27]–[29]. Taking inner product for example, for each feature vector $x \in T.X$, we perform an inner product $w^T x$ as part of the inference computation, where w is a weight matrix. Since T has redundant tuples, redundant inner product computation will occur, which can be avoided by factorizing the inner products over $x \in X$ into inner products over the feature vectors $x_R \in X_S$ and $x_R \in X_R$, leveraging $w^T x = w_S^T x_S + w_R^T x_R$, wherein w_S/w_R is the projection of w to the

features from S/R . Pushing $w_S^T x_S$ down to table S and pushing $w_R^T x_R$ down to table R will avoid redundant computations caused by the join.

R2-2 Factorization of Decision Tree Inference [110], [111]. A k -depth decision tree f contains 2^{k-1} leaf nodes and $2^{k-1} - 1$ intermediate nodes. Each intermediate node is associated with a feature in the input $x \in T.X$, and outputs True/False based on the feature's value. Intermediate nodes are divided and pushed down to R or S based on whether their features are from R or S . The detailed factorized inference process is based on the QuickScorer algorithm [110], [111] that encodes each intermediate node into a 2^{k-1} -length bit vector and converts the decision tree inference result into the bitwise AND of the bit vectors of all False nodes (i.e., intermediate tree nodes that return False on the input feature). The bitwise AND computations can be performed on R and S respectively, and then aggregated.

R2-3 Factorization of Distance Computation [9]. If each feature vector $x \in X$ needs to compute a Euclidean distance with a vector of same length called y , i.e., $dist(x, y)$, we can avoid redundant computation on repeated tuples in T by factorizing the distance computation into $dist(x_S, y_S)$ and $dist(x_R, y_R)$, wherein y_S/y_R is the projection of y to the features from S/R , and pushing down them to S and R respectively, leveraging $dist(x, y) = \sqrt{dist^2(x_S, y_S) + dist^2(x_R, y_R)}$.

O3. Tensor-Relational Transformation. The computation abstraction consists of a limited set of tensor-relational operators [30], such as `aggregate`, `join`, `crossJoin`, `filter`, `project`, `rekey`, `tile`, `concat`, all processing relations. In the data abstraction, the model parameters must be transformed into relations (as discussed in R3-1 to R3-3). Example co-optimization techniques include:

(Notations: similar to the notations in O2, $T(Y, X)$ is a relation, where X is a column of feature vectors.)

R3-1 Linear algebra operators transformed to relational operators [30], [55]–[57]. To enable the transformation, a matrix w could be transformed into a relation $R(colId, tile)$, where each tuple represents a vertically partitioned matrix tile indexed by $colId$, with its data flattened in a 1-D array in the $tile$ attribute. Then taking `matMul` between feature vectors in $T.X$ and w as an example, it can be converted into a `crossJoin` followed by `project`. The `crossJoin` pairs each feature vector in T with each tile in R . Then each joined pair of $x \in T.X$ and $t \in R.tile$ is applied with a `project` that computes $x \times t$. An output block has its row index being the feature vector's row index and its column index being the tile's column index. As described in Tensor Relational Algebra (TRA) [30], other linear algebra computations can also be represented in relational algebra.

R3-2 Decision Forest, e.g., XGBoost and lightGBM, to crossJoin, project, and aggregate [20]. A decision forest model can be represented as a relation $DF(TreeId : INT, TreeObj : TreeType)$, where each tuple represents a decision tree indexed by $TreeId$, and stored as a tree object in the $TreeObj$ column. Applying the model to each feature vector $x \in T.X$, could be transformed into relational processing by first performing a `crossJoin` of T and DF . Then a `project` is applied to each joined pair of $x \in T.X$ and $t \in DF$ to run $t.predict(x)$. Furthermore, the prediction results are aggregated to obtain the final prediction.

R3-3 distances_to_centroids to crossJoin and project. Given a set of clusters represented in a relation $R(ClusterId, C)$, where each tuple represents a cluster indexed by $ClusterId$ with centroid c in the C column. Computing the distance of each feature vector $x \in T.X$ with each centroid $c \in R.C$ can be represented as a `cross_join` of T and R , followed by a `project` that computes the distance between $c \in R.C$ and $x \in T.X$.

The O3 transformations scale to AI/ML models that involve large-scale parameters, by blocking the parameters so that each time only a few blocks need to be loaded into the memory (via buffer pool management). However, such transformation increases overheads for AI/ML models with small parameters [12].

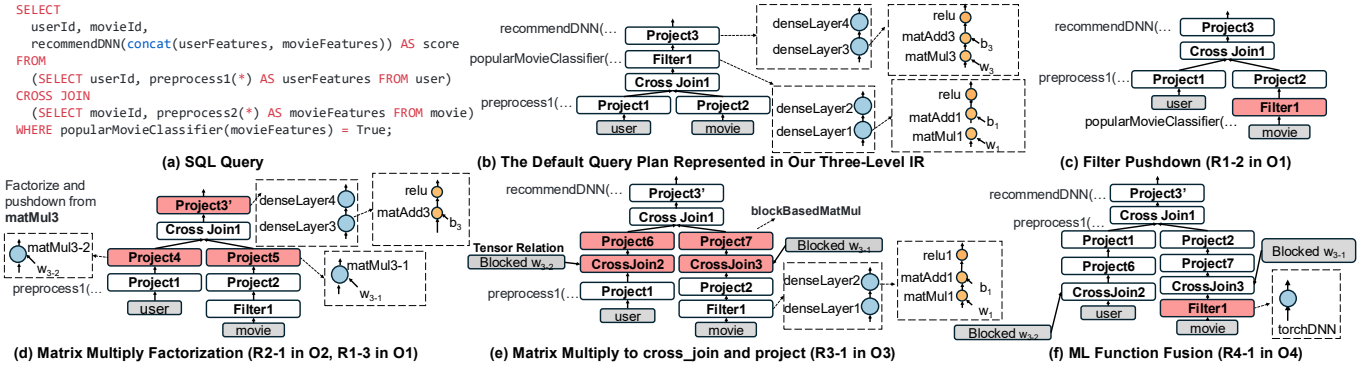


Fig. 12: A Variant Example of Our Three-Level IR.

Finally, as shown in Fig. 12(f), it applies R4-1 to fuse all operators in the popularMovieClassifier model into one high-level ML function that invokes the torchDNN library.

C. Weisfeiler-Lehman Encoding Process

In this section, we describe how the Weisfeiler-Lehman (WL) kernel is applied to construct positive and negative training samples. The WL kernel encoding procedure is outlined in Algorithm 6. It iteratively generates feature vectors by aggregating and updating node labels. While the encoding processes of Model2Vec and Query2Vec are largely similar, they differ in how the initial node labels are assigned. In Model2Vec, the initial labels are determined by the kernel’s FLOPs values. In contrast, Query2Vec assigns initial labels based on different strategies tailored to each node type. These initialization procedures are detailed in Algorithm 7 and Algorithm 9, respectively.

Algorithm 6: Weisfeiler-Lehman Kernel Feature Extraction

```

Input : root: root node of the model tree
          T: number of WL iterations
Output:  $\mathcal{F}$ : WL subtree feature counts
1  $\mathcal{L}, \mathcal{H}, \mathcal{N} \leftarrow \emptyset$ ; // Label map, history, node list
2 DFS(root,  $\mathcal{L}, \mathcal{H}, \mathcal{N}$ ); // Initialize the labels through DFS
3 for  $i \leftarrow 1$  to  $T$  do
4    $\mathcal{L}_{new} \leftarrow \emptyset$ ;
5   foreach  $node \in \mathcal{N}$  do
6      $C \leftarrow \text{sorted}([\mathcal{L}[c] \mid c \in \text{node.children}]);$ 
7      $label_{new} \leftarrow \mathcal{L}[node] + C$ ;
8      $\mathcal{L}_{new}[node] \leftarrow label_{new}$ ;
9      $\mathcal{H}[node].\text{append}(label_{new})$ ;
10   $\mathcal{L} \leftarrow \mathcal{L}_{new}$ ;
11  $\mathcal{F} \leftarrow \emptyset$ ; // Feature vector
12 foreach  $node \in \mathcal{N}$  do
13   foreach  $label \in \mathcal{H}[node]$  do
14      $\mathcal{F}[label] += 1$ ;
15 return  $\mathcal{F}$ 

```

D. Error Bound Analysis via (p, q) -Consistency

We model query optimization as a discounted MDP $M = (\mathcal{S}, \mathcal{A}, P, R, \gamma)$, where states are query plans and actions are configurable rewrite-rule instantiations. Let $V^*(s)$ and $Q^*(s, a)$

Algorithm 7: Initial Node Label Assignment for Model2Vec

```

Input : node: a tree node with operator type and FLOPs
           $\mathcal{G}$ : label groups by kernel type
           $\rho$ : FLOPs range threshold
Output: label: unique label assigned to the node
1  $type \leftarrow \text{node.ml\_op\_type}$ ;
2  $flops \leftarrow \text{node.ml\_op\_flops}$ ;
3  $group \leftarrow \mathcal{G}[type]$ ;
4  $idx \leftarrow \text{BinarySearchWithRange}(group, flops, \rho)$ ;
5 if  $idx = -1$  then
6    $label \leftarrow t_f$ ;
7    $group.\text{append}(flops)$ ;
8    $group.\text{sort}()$ ;
9    $\mathcal{G}[type] \leftarrow group$ ;
10 else
11    $label \leftarrow type + group[idx]$ ;
12 return label

```

Algorithm 8: DFS Traversal for Label Initialization

```

Input : root: root node of the model tree
           $\mathcal{L}$ : node label map
           $\mathcal{H}$ : node label history
           $\mathcal{N}$ : list of all nodes
Output: Updated  $\mathcal{L}, \mathcal{H}$ , and  $\mathcal{N}$ 
1 Function DFS( $node, \mathcal{L}, \mathcal{H}, \mathcal{N}$ ):
2    $label \leftarrow \text{InitialNodeLabel}(node)$ ;
3    $\mathcal{L}[node] \leftarrow label$ ;
4    $\mathcal{H}[node] \leftarrow [label]$ ;
5    $\mathcal{N}.\text{append}(node)$ ;
6   foreach  $child \in \text{node.children}$  do
7     DFS( $child, \mathcal{L}, \mathcal{H}, \mathcal{N}$ );

```

be optimal values, and define the (root) simple regret for the input state s_0 :

$$\mathcal{R}(s_0) = V^*(s_0) - Q^*(s_0, \hat{a}) = \max_{a \in \mathcal{A}(s_0)} Q^*(s_0, a) - Q^*(s_0, \hat{a}), \quad (7)$$

where \hat{a} is the action returned by CACTUSDB after B_{iter} simulations.

The query embedding process $f: \mathcal{S} \rightarrow \mathcal{X}$ is a subjective function mapping ground states \mathcal{S} to their equivalence classes (i.e., abstract states representing clusters of query plans that share the same query embedding) in \mathcal{X} . Then, given a logical query plan s_0 , we view the optimization problem as a Markov Decision Process (MDP) $\langle \mathcal{T}, \mathcal{A}, \mathcal{P}, \mathcal{R} \rangle$ on trajectories, with action space \mathcal{A} , state space $\mathcal{T} = \{s_0\} \times (\mathcal{A} \times \mathcal{S})$ being the

Algorithm 9: Initial Node Label Assignment for Query2Vec

Input : node: a tree node with type and model embedding
 \mathcal{G} : label groups by node type
 \mathcal{I} : FAISS model embedding index
 τ : similarity threshold

Output : label: label assigned to the node

```

1 type ← node.nodeType;
2 group ←  $\mathcal{G}[t]$ ;
3 if node.hashML then
4   q ← normalize(e);
5   idx, sim ←  $\mathcal{I}$ .search(node.mlEmbed);
   // Assign label based on embedding
   similarity
6   if sim >  $\tau$  then
7     label ← type + idx
8   else
9     label ← type + next_idx;
10     $\mathcal{I}$ .add(node.mlEmbed);
11    next_idx ← next_idx + 1;
   // Assign label based on relation data
12 else if type = TableScanNode then
13   label ← t + node.table_id;
   // Assign label based on filter predicate
14 else if type = FilterNode then
15   c ← node.filter["colId"];
16   o ← node.filter["opId"];
17   v ← node.filter["val"];
18   label ← t + c + o + v;
   // Assign label based on project expression
19 else if type = ProjectNode then
20   label ← t + node.projectExpr;
   // Assign label based on join predicate
21 else if type ∈ {HashJoinNode, NestedLoopJoinNode} then
22   label ← t + node.join;
   // Assign label based on aggregation keys
23 else if type = AggregationNode then
24   label ← type + node.aggKeys;
25 else
26   label ← type;
27 group.add(label);
28 return label

```

collection of any state-action sequence of any length that starts in s_0 within a length bound d . The transition matrix $\mathcal{P}(t, a, t') = \mathcal{P}(s, a, s')$, which represents that the transition probability of t to t' (one step extension of t) for $a \in \mathcal{A}$ equals to the transition probability of ground state transitioning s to s' for a , where s is the last state in the trajectory t , and s' is t' 's one-step extension in t' . We also have $\mathcal{R}(t)$ denoting the reward of selecting s to form trajectory t . The Q function and the value function at trajectory t is defined as usual:

$$Q^*(t, a) = \mathcal{R}(t) + \sum_{t' \in \mathcal{T}} P(t, a, t') V^*(t') \quad (8)$$

$$V^*(t) = \max_{a \in \mathcal{A}} Q^*(t, a) \quad (9)$$

We then define the application of query embedding f to each ground state s in $t \in \mathcal{T}$, such that $f(t) = f(s_0)a_1f(s_1) \dots a_kf(s_k)$. Then, under f , we can define the space of abstracted trajectories at the query embedding level, denoted as $\mathcal{H} = \{h \in \{t_0\} \times (\mathcal{A} \times f) : |h| \leq d\}$. Hence, \mathcal{H}

forms partition of \mathcal{T} . Then, following existing works on MCTS with state aggregation [81], it is easy to prove the following theorem regarding the error bound of the Q function in our proposed optimization process:

Theorem 2 (reusable MCTS error bound under (p, q) -consistency). Assume our query embedding process f satisfies (p, q) -consistency for $p, q \geq 0$ such that for all $h \in \mathcal{H}$,

$$\exists a^* \in \mathcal{A} : V^*(t) - Q^*(t, a^*) \leq p \quad \forall t \in h \quad (10)$$

$$|V^*(t_1) - V^*(t_2)| \leq q \quad \forall t_1, t_2 \in h. \quad (11)$$

Then, the optimal action in the MCTS tree with state abstraction by f , $a^* = \arg \max_{a \in \mathcal{A}} Q^*(h_0, a)$, has Q^* error in the root state bounded by

$$|\max_{a \in \mathcal{A}} Q^*(s_0, a) - Q^*(s_0, a^*)| \leq 2d(p + q) \quad (12)$$

E. Proof of Theorem 2

1) Expectimax-tree abstraction and (p, q) -consistency:

We briefly restate the abstract expectimax-tree construction (specialized to our notation). Let \mathcal{H} be the history partition induced by f , and let $\mu = \{\mu_h\}$ be a family of distributions over ground trajectories $t \in h$. The induced abstract-tree transition is

$$\mathcal{P}_\mu(h, a, h') = \sum_{t \in h} \mu_h(t) \sum_{t' \in h'} \mathcal{P}(t, a, t'),$$

and the abstract value functions satisfy the standard Bellman optimality equations on the history tree:

$$Q_\mu^*(h, a) = \mathcal{R}_\mu(h) + \sum_{h' \in \mathcal{H}} \mathcal{P}_\mu(h, a, h') V_\mu^*(h'), \quad (13)$$

$$V_\mu^*(h) = \max_{a \in \mathcal{A}} Q_\mu^*(h, a), \quad (14)$$

where $\mathcal{R}_\mu(h) = \sum_{t \in h} \mu_h(t) \mathcal{R}(t)$ (see [81]).

We assume (p, q) -consistency, i.e., for each $h \in \mathcal{H}$ there exists a_h^* such that (10)–(11) hold. This matches the definition in [81].

2) *Optimal weighting μ^* and one-step divergence:* In expectimax-tree abstractions, correctness depends not only on f but also on how probability mass is assigned to the ground trajectories inside each history. Hostetler et al. define an *optimal* weighting μ^* and measure deviation from it via a one-step divergence quantity; we reuse that notion here. Let $m \triangleq \max_{h \in \mathcal{H}} \delta(\mu, h) \leq 1$ be the maximum single-step divergence (notation and formal definition as in [81]). When reusable MCTS/UCT aggregates statistics by sampling ground transitions and mapping them to histories, it behaves as if it were using μ^* in the abstract tree (under the conditions discussed in [81]); in the most conservative setting we only assume $m \leq 1$.

3) *Key error decomposition and induction:* Fix any history node h and action a . Define the action-value estimation error

$$E(h, a) \triangleq \left| Q_\mu^*(h, a) - \sum_{t \in h} \mu_h(t) Q^*(t, a) \right|.$$

Following the proof strategy in [81], decompose the error into (i) error propagated from deeper abstract values and (ii) error introduced by aggregating/weighting at the current step:

$$E(h, a) \leq E_Q(h, a) + E_\delta(h, a),$$

where E_Q captures the mismatch between $V_\mu^*(\cdot)$ and the weighted ground optimal values below children, and E_δ captures the single-step weighting/aggregation deviation at the current expansion.

The proof proceeds by induction on the remaining depth k to leaves (base case holds at terminal/absorbing nodes). Assume the inductive hypothesis

$$E(h', a) \leq k(p+mq) \quad \text{for all children } h' \text{ of } h \text{ and all } a \in \mathcal{A}.$$

Using (p, \cdot) -consistency (which allows exchanging max and \sum with additive penalty p) plus the inductive hypothesis yields

$$E_Q(h, a) \leq k(p + mq) + p.$$

This corresponds to the step “exchange max and sum at cost $\leq p$ ” in [81].

For the single-step abstraction error, (\cdot, q) -consistency implies that within any child history the optimal values vary by at most q , and the deviation of μ from μ^* scales this by at most the one-step divergence. This yields

$$E_\delta(h, a) \leq mq,$$

as in the convex-combination argument in [81].

Combining gives the inductive step:

$$E(h, a) \leq (k + 1)(p + mq).$$

Thus at the root history h_0 (depth d), for any action a we have $E(h_0, a) \leq d(p + mq)$.

4) *From value-estimation error to root action suboptimality:* Let $a^\# \in \arg \max_a Q_\mu^*(h_0, a)$ be the abstract-tree optimal action, and let $a^* \in \arg \max_a Q^*(s_0, a)$ be the ground-tree optimal root action. In the worst case, the abstract estimate overvalues $a^\#$ by at most $d(p + mq)$ and undervalues a^* by at most $d(p + mq)$, yielding

$$Q^*(s_0, a^*) - Q^*(s_0, a^\#) \leq 2d(p + mq).$$

This is exactly the final root-step argument in [81]. Since $m \leq 1$, we also obtain the simplified bound $2d(p + q)$. \square

F. GPU Acceleration

Further discussion: GPU Support While this work focuses on CPU, our reusable MCTS optimizer is aware of the equivalence between CPU and GPU implementation of the same ML function and leverages R4-2 to invoke LibTorch CUDA library [112] in our GPU environment (see the beginning of Sec. V). As shown in Tab. III, GPU offloading achieved by our optimizer yields an additional 17%–55% performance improvement over the optimized query plan and accelerates model inference by 1.3 \times on average. However, fully optimizing GPU acceleration raises challenges in pipelining, load balancing, and CPU–GPU

coordination. These aspects are beyond the scope of this paper and are left for future work.

TABLE III: Recommendation Query Performance with GPU Enabled

	EvaDB	Apache PySpark w/UDF	DL-Centric	CactusDB	
				w/o GPU Extension	w/ GPU Extension
Q1	40.40 sec	48.56 sec	47.2 sec	0.14 sec	0.09 sec
Q2	Failed (OOM)	Failed (OOM)	119.54 sec	2.71 sec	2.14 sec
Q3	Failed (OOM)	Failed (OOM)	172.39 sec	18.67 sec	15.93 sec

G. Extended Related Works

In-DB AI/ML Systems. To the best of our knowledge, no existing system fully supports all categories of SQL-ML co-optimization techniques (O1–O4). UDF-centric systems such as EvaDB [10] and PostgresML [11] support most O1 techniques by allowing inference logic to be encapsulated in user-defined functions. MADLib [24] and PySpark [99] provide partial support for O1, but handle arbitrary UDFs poorly. For instance, MADLib cannot push down table-level UDFs like *madlib.mlp_classification*, and PySpark only pushes down MLlib functions and not arbitrary UDFs. These systems cannot analyze or transform UDF internals, making them unsuitable for deeper co-optimization as required by O2–O4. Existing factorized ML systems [26]–[29], [54], [100] focus on ML training processes, relying on predefined factorizable AI/ML models or linear algebra (LA) operators. Although related to O2-style optimization, they lack dynamic decomposition of arbitrary inference pipelines and integration with O3/O4 type optimizations. IMBridge [64], [97] optimizes query performance through automated ML inference context caching and batch inference. Nonetheless, it lacks support for O2 and O3, which are essential for comprehensive end-to-end performance optimization. Other systems like SimSQL [31], [55], SystemML [56], and SystemDS [89] embed ML workloads in relational algebra atop big data processing platforms like Hadoop [113] or Spark [114]. MASQ [41], [101] rewrites limited inference operators (e.g., one-hot encoding, linear models, decision trees) into SQL. None explore partial translation of LA operators into relational form for O2/O4 co-optimization.

Intermediate Representations (IRs). Several unified IRs have been proposed for SQL-ML co-optimization, though most cover only subsets of O1–O4. Raven [38] combines relational, LA, and ML operators, supporting O1 and O4 and partially O3 by converting full ML pipelines into relational form, reducing flexibility. SDQL [60] uses a semi-ring IR covering O1, O2, and O4, but cannot transform LA into relational operators (lacking O3). Weld [36] unifies computation across libraries through vector operators (e.g., *vecbuilder*, *vecmerger*), enabling fusion and data-movement optimization, yet most O1–O3 techniques must be implemented outside of the IR [37]. Lara [59] uses monad comprehensions for UDFs, enabling O1/O4 optimizations (push-down, layout tuning) but not O2/O3. LingoDB [102], [103] leverages MLIR for combining relational and non-relational workloads (e.g., *k-means*, *PageRank*) [115]. While flexible, it does not target SQL-ML co-optimization techniques in O2–O4. Tensor Relational Algebra [30] primarily addresses O3-style integration of tensors with relational queries, without broader support for O1, O2, or O4.

Inference Query Optimization. Raven [38] applies logical optimizations in a fixed order using rule-based, classification, and regression strategies to choose among ML2SQL, ML2DNN, or no optimization. Most other in-database AI/ML systems rely on rules and heuristics for inference query optimization. Weld [36] and Lara [59] use rule-based plan selection, while SDQL [48] applies rewrite rules until reaching a fixed point.

Database query optimization has evolved into a multifaceted research domain, encompassing rule-based, cost-based, and learning-based approaches. **Rule-based optimizers (RBOs)** apply predefined transformations (e.g., Spark Catalyst [104], [105]), but fixed ordering can yield suboptimal plans. **Cost-Based Optimizer (CBO)** [106]–[108] estimates the cost of query execution using statistical models and employs techniques such as dynamic programming, genetic algorithms, and Monte Carlo Tree Search (MCTS) [43], [46]. **Learned optimizers (LBOs)** [9], [43], [69], [109] use ML for cost or cardinality estimation but struggle with ad-hoc AI/ML queries unseen during training.

Our Work. To close the gaps, we proposed CACTUSDB, a novel in-database AI/ML system focusing on inference queries. Like Raven [38], and different from Weld [36], Lara [59], LingoDB [103], and SDQL [60], CACTUSDB allows relational, linear-algebra, and ML operators to co-exist for expressive and flexible query processing. But our system is distinct from Raven in the following aspects: (1) Unlike Raven’s ONNX-based IR, CACTUSDB encodes AI/ML semantics using native database expressions in UDF-centric systems, forming a three-level IR. This yields tighter integration with existing optimizers, improved partial evaluation, and seamless adoption in SQL/UDF systems. (2) Instead of treating ML pipelines as monolithic graphs, CACTUSDB decomposes inference pipelines into fine-grained sub-computations, enabling selective optimizations such as factorization, push-down, and tensor-relational conversion. (3) While Raven explores a small rule-based search space (ML2SQL, ML2DNN, or none), CACTUSDB introduces a new optimizer combining query embeddings with MCTS to efficiently search the exponentially large space of co-optimization strategies.

H. Vanilla MCTS Algorithm

The Alg. 10 describes how the vanilla MCTS algorithm is used in query optimization.

I. Recommendation Queries

The three recommendation queries we used in evaluation are described in List. 1 based on the MovieLens dataset, with the corresponding ER diagram shown in Fig. 13.

In Q1, the trending model has an input size of 3, with hidden layers of 128 and 64 units. ReLU is used as the activation function. The output layer consists of a single neuron with a sigmoid function. The two tower model initialized embedding tables of dimension 32 for each categorical feature. Later, the concatenated user and movie features are then passed to a fully connected neural network with the two hidden layers, each containing 300 neurons. The output layer consists of 128

Algorithm 10: General MCTS Algorithm

Input: *root*, the state of the original query plan; *B_{iteration}*, the budget of MCTS training iterations

```

1 for i in range(Biteration) do
2   node ← root;
   /* If the current node is fully expanded,
   perform node selection. Otherwise,
   perform node expansion. */
3   while node.isTerminalState() == False do
4     if node.expanded then
5       node ← select(node);
6     else
7       node ← expand(node);
8       node' ← rollout(node);
9       break;
10  reward ← computeReward(node');
11  backpropagate(node, reward);
12 return;
```

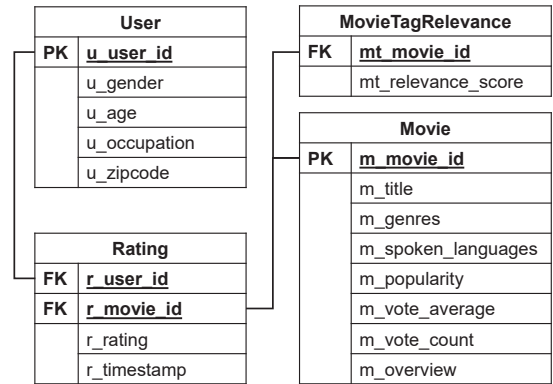


Fig. 13: ER Diagram of MovieLens Database

neurons. The input features dimensions are 129 for each user and 65 for each movie.

In Q2, the trending model is the same as the one used in Q1. The *predict_user_interest_DNN* is a fully connected neural network with an input dimension of 259 and a single hidden layer containing 128 neurons. Its output consists of two neurons with a softmax activation function. The Autoencoder model takes an input of size 140,979, representing the number of unique movie tags, with a hidden layer of 2,048 neurons. The output is a dense layer with 256 neurons. The DLRM model initializes embedding tables of dimension 128 for each categorical variable. The numerical features are processed by a one-layer MLP, a fully connected neural network with an input size of 256 and output size of 128. The categorical features’ embedding vectors are concatenated with the MLP’s output and then passed to another one-layer MLP, with an input size of 256, a hidden layer of 128 neurons, and a single-neuron output layer.

In Q3, *autoencoder* and *predict_user_interest_DNN* are both fully connected neural networks with the same architecture as described in Q2. *predict_rating_DNN* is another fully connected neural network, which has an input dimension of 5, two hidden layers with 512 and 1024 neurons, respectively, and an output layer of size 6.

```

1 // Q1
2 SELECT
3   two_tower_model (user_feature, movie_feature)
4 FROM
5   (
6     SELECT
7       concat(embedding (user_id), embedding (
8         gender), embedding (age), embedding (
9         occupation), user_avg_rating) AS
10      user_feature
11 FROM
12   USER u
13   JOIN (
14     SELECT user_id, average (rating) AS
15     user_avg_rating
16     FROM rating GROUP BY user_id
17   ) ON u.user_id=user_id
18 )
19 CROSS JOIN (
20   SELECT
21     concat(embedding (movie_id), embedding (
22     genres), movie_avg_rating) AS
23     movie_feature
24 FROM
25   movie m
26   JOIN (
27     SELECT movie_id, average (rating)
28     FROM rating GROUP BY movie_id
29   ) ON m.movie_id=movie_id
30 WHERE
31   movie.genres LIKE '%Action%' AND
32   trending_movie_DNN(movie_feature)=1
33 )
34 // Q2
35 SELECT
36   DLRM(user_feature,movie_feature,
37   movie_dense_feature)
38 FROM
39   (SELECT
40     feature_extraction1(*) AS user_feature
41 FROM
42   user
43   CROSS JOIN (
44     SELECT
45     feature_extraction2(movie_feature),
46     autoencoder(movie_relevance_tag) AS
47     movie_dense_feature
48 FROM
49   movie
50   JOIN movie_tag_feature ON movie.
51     m_movie_id=movie_tag_feature.
52     mt_movie_id
53 )
54 WHERE
55   predict_trending_movie_DNN(movie_feature
56   )=1
57   AND predict_user_interest_DNN(
58     user_feature, movie_dense_feature)
59   =1)
60 // Q3
61 SELECT
62   cosine_similarity(movie_dense_feature1,
63   movie_dense_feature2) AS relevant_score

```

```

64 FROM
65   (
66     SELECT
67     autoencoder(mt_relevance_score) AS
68     movie_dense_feature1
69 FROM
70   (
71     SELECT
72     preprocess1(user.*) AS user_feature,
73     preprocess2(movie.*) AS
74     movie_feature
75 FROM
76   user
77   CROSS JOIN movie
78   JOIN movie_tag_relevance ON mt.
79     movie_id = m_movie_id
80 )
81 WHERE
82   genres LIKE '%Fiction%'
83   AND predict_user_interest_DNN(
84     user_feature, movie_feature) = 1
85   AND predict_rating_DNN(user_feature,
86     movie_feature) > 3
87 )
88 CROSS JOIN(
89   SELECT
90     autoencoder(mt_relevance_score) AS
91     movie_dense_feature2
92 FROM
93   movie_tag_relevance

```

Listing 1: Query 1

J. Retailing-Complex Queries

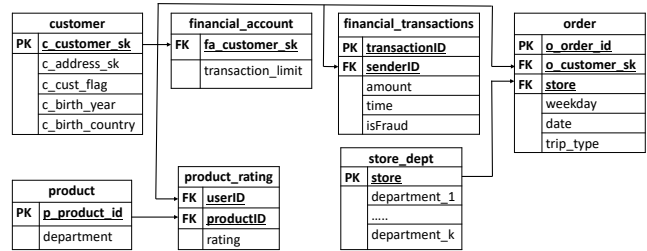


Fig. 14: Simplified ER Diagram of Retailing Dataset from TPCx-AI [116]

List. 2 presents three complex queries based on the TPCx-AI dataset, with the corresponding ER diagram shown in Fig. 14.

In Q1, `is_popular_store` is a UDF that computes a popularity score for each store based on its department availability. `trip_classifier_dnn` is a neural network comprising a customer embedding table and a fully connected neural network. The embedding table is initialized with the dimension of 16, and the resulting customer embedding vector is concatenated with additional features, forming an input of size 63. The input is then passed through a fully

connected neural network with two hidden layers of 48 and 24 neurons, respectively, followed by an output layer of size 1000, representing the trip types.

In Q2, `dnn_fraud_predict` is a deep neural network (DNN) model designed for fraud classification, consisting of an input layer of size 32, a single hidden layer with 12 neurons, and an output layer of size 2. `xgboost_fraud_predict` is an XGBoost model with 1,600 trees which take 5 features.

Q3 invokes a two-tower model that initializes multiple embedding tables for categorical variables, each with a dimension of either 16 or 8. Customer features and product features are processed separately through the user tower and product tower. The user tower is a fully connected neural network with an input size of 50, followed by two hidden layers with 128 and 64 neurons and an output layer of 16 neurons. The product tower has a similar structure but with a different input size of 25.

```

1 // Q1
2 SELECT o_order_id, trip_classifier_dnn (concat
3   (order_feature, store_feature))
4 FROM (
5   SELECT o_order_id , get_order_features(
6     o_customer_sk, weekday, date) AS
7     order_feature, store_feature
8 FROM order o
9 JOIN (
10    SELECT store, concat (*) AS store_feature
11    FROM store_dept_wide s
12  ) ON o. store = s.store
13 WHERE o. weekday != 'Sunday' AND
14    is_popular_store (store_feature) = 1
15 )
16
17 // Q2
18 SELECT transactionID
19 FROM (
20   SELECT c_customer_sk , get_customer_feature
21     (c_address_sk, c_cust_flag, c_birth_year
22     , c_birth_country, transaction_limit) AS
23     customer_feature
24 FROM customer
25 JOIN (
26   SELECT fa_customer_sk, transaction_limit
27   FROM financial_account
28 ) ON c_customer_sk = fa_customer_sk
29 WHERE c_cust_flag = 0
30 JOIN (
31   SELECT transactionID, senderID,
32     get_transaction_feature (*) AS
33     transaction_feature
34 FROM financial_transactions t
35 ) ON c_customer_sk = senderID
36 WHERE age_during_transaction ( c_birth_year
37   , t.time) >= 18 AND is_working_day (t.
38   time) = 1
39 )
40 WHERE xgboost_fraud_predict(concat (
41   customer_feature, transaction_feature)) >=
42   0.5 AND dnn_fraud_predict(concat (
43   customer_feature, transaction_feature)) =
44   1
45

```

```

32 // Q3
33 SELECT two_tower_model (customer_feature,
34   product_feature)
35 FROM (
36   SELECT concat(embedding (c_customer_sk),
37     embedding (c_address_sk), c_cust_flag,
38     embedding (get_age (c_birth_year)),
39     embedding (birth_country),
40     customer_avg_rating) AS customer_feature
41 FROM customer c
42 JOIN (
43   SELECT userID, AVG (rating) AS
44     customer_avg_rating
45 FROM product_rating GROUP BY userID
46 ) AS cr ON c. c_customer_sk = cr.userID
47 ) AS customer_outer
48 CROSS JOIN (
49   SELECT concat(embedding (p_product_id),
50     embedding(department),
51     product_avg_rating) AS product_feature
52 FROM product p
53 JOIN (
54   SELECT productID, AVG (rating) AS
55     prod_avg_rating
56 FROM product_rating GROUP BY productID
57 ) AS pr ON p. p_product_id = pr.productID
58 WHERE pr.prod_avg_rating >= 4.0
59 ) AS prod_outer

```

Listing 2: Queries on Retailing Dataset

K. LLM Queries

List. 3 describes the two LLM queries used in our evaluation. We utilize OpenAI’s RESTful API to invoke the `gpt-3.5-turbo` model to summarize the user/movie information and make the recommendations. The `trending_movie_classifier` is a fully connected neural network with the same structure as the one described in Sec. I. Q2 employs a RAG-based approach to retrieve movies’ relevant information by performing a nearest-neighbor vector search on pre-built document embedding vectors using Faiss’s cosine similarity index.

```

1 // Q1: Using LLM for Movie Recommendation
2 SELECT LLM('Please give a recommendation score
3   and explain why', LLM('Please summarize',
4   u.description), LLM('Please summarize', m.
5   .description))
6 FROM user u CROSS JOIN movie m
7 WHERE m.spoken_language LIKE % English % AND
8   trending_movie_classifier(m.popularity, m.
9   vote_average, m.vote_num) = True;
10
11 // Q2: Using RAG to retrieve relevant
12 information with given movie title and
13 using LLM for recommendation
14 SELECT LLM('Please give a recommendation score
15   and explain why', LLM('Please summarize',
16   u.description), RAG(m.title))
17 FROM user u CROSS JOIN movie m
18 WHERE m.spoken_language LIKE % English % AND
19   trending_movie_classifier(m.popularity, m.
20   vote_average, m.vote_num) = True;

```

Listing 3: LLM Queries

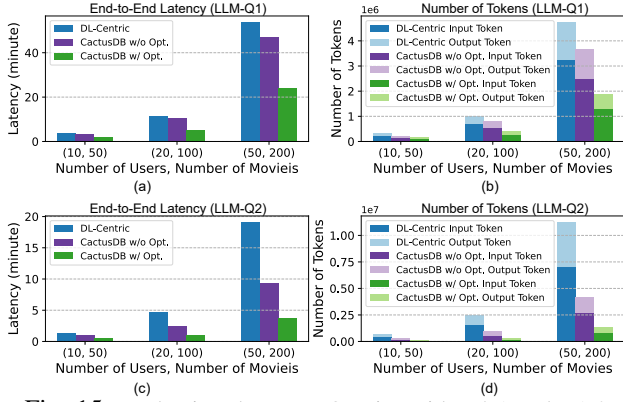


Fig. 15: Evaluating the LLM Queries with R4-1 and R1-3

LLM Inference Queries. In this benchmark, the overheads of LLM inferences dominate the end-to-end latency. In addition, the monetary costs of LLM usage linearly increase with the number of tokens sent to and received from LLM. Q2 replaces the LLM-based movie summarization with RAG, which results in faster execution but increases the number of tokens compared to Q1. As shown in Fig. 15, **our CACTUSDB is capable of factorizing the nested LLM functions and pushing down the LLM summarization call and RAG call before the cross_join to avoid repeatedly LLM inferences on the same records, resulting in 3× speed up and 72.4% reduction of tokens (and costs) on average.** We noticed that even without enabling our reusable MCTS query optimizer, CACTUSDB benefits from Velox’s built-in runtime optimization, such as filter push-down. These runtime optimizations effectively reduced the total number of input/output tokens sent to the LLMs by 25% for Q1 and 59% for Q2 on average with end-to-end latency speedups of 1.1× to 2.1×.

L. Comparison of Optimization Algorithms on Recommendation Queries

TABLE IV: Comparison of Optimization Algorithms (unit: second)

	Recommendation-Q1			Recommendation-Q2			Recommendation-Q3		
	Opt.	Exec.	Total	Opt.	Exec.	Total	Opt.	Exec.	Total
Un-optimized	NA	144.2	144.2	NA	13.6	13.6	NA	36.5	36.5
Arbitrary	0.9	1.8	2.7	5.1	131.3	136.3	4.4	23.7	28.1
Heuristic	0.2	5.2	5.4	0.3	12.3	12.6	0.1	16.3	16.3
Vanilla MCTS	5.2	0.3	5.5	6.8	6.8	13.6	10.3	8.7	18.9
Reusable MCTS	1.5	0.2	1.7	2.1	6.5	8.6	3.6	8.8	12.4

Recommendation queries. We break down the end-to-end latency of each query into two parts: query optimization latency and query execution latency. Tab. IV compares the latency for query optimization (Opt.), query execution (Exec.), and the total of them. **Our reusable MCTS strikes the best trade-off between overhead and effectiveness compared to other baselines. Even though it introduces additional overhead for query embedding, the query optimization latency is greatly saved by reusing the MCTS.** The arbitrary optimization strategy could lead to better or worse query execution time

compared to unoptimized queries. That is because not all optimization rules will be beneficial. Heuristic optimization strategy will always lead to better efficiency (optimization latency). However, simply relying on pre-defined heuristics cannot exploit the best optimization techniques for all queries. Vanilla MCTS demonstrates effectiveness in searching for optimal query plans due to its query-specific optimization. However, it requires building an MCTS search tree from scratch every time, which worsens the optimization latency.

M. Synthetic Model Sampling

We design a model sampling strategy to generate diverse architectures for collecting the training data for the Model2Vec model. The strategy is built on a set of reusable model-building blocks, which we denote as parameterized operators:

- ConvolutionalLayer (in, out, kernel, stride, padding)
- PoolingLayer (kernel, stride, padding)
- LinearLayer (in, out, activation, bias)
- BatchNormalization (num_features, ϵ)
- Dropout(p)
- EmbeddingLayer (num_tuples, dim)
- SVD (dim)
- Decision_Forest (n_{trees} , d_{max})
- DecisionTree (d_{max})
- Activation \in {ReLU, Sigmoid, Tanh, Softmax}
- Concat (\cdot)
- CosineSimilarity (\cdot, \cdot)
- Flatten (\cdot)

Each operator can be parameterized within a configurable range, and blocks may be repeated between a minimum and maximum depth. Using these primitives, users can compose customized model templates based on their needs. In our work, we define a set of representative model templates, which are used to generate training data, as illustrated in List. 4:

```

1 // Multi-Layer Perceptron (MLP)
2 MLP :=
3   Repeat{min_repeat, max_repeat}{
4     LinearLayer(RANGE(in_min, in_max),
5                 RANGE(out_min, out_max),
6                 CHOICE(Activation))
7   }
8 // Two-Tower Model
9 Tower :=
10  Repeat{min_repeat, max_repeat}{
11    LinearLayer(RANGE(in_min, in_max),
12               RANGE(out_min, out_max),
13               CHOICE(Activation))
14  }
15 TwoTowerModel := CosineSimilarity(Tower, Tower)
16 // Deep Learning Recommendation Model (DLRM-style)
17 DLRM :=
18  Concat(
19    Repeat{min_repeat, max_repeat}{
20      EmbeddingLayer(RANGE(num_min, num_max),

```

```

23         RANGE(dim_min, dim_max))
24     ),
25     Repeat{min_repeat, max_repeat}(
26         LinearLayer(RANGE(in_min, in_max),
27                     RANGE(out_min, out_max),
28                     CHOICE(Activation))
29     )
30 )
31 -> Repeat{min_repeat, max_repeat}(
32     LinearLayer(RANGE(in_min, in_max),
33                 RANGE(out_min, out_max),
34                 CHOICE(Activation))
35 )
36
37 // Convolutional Neural Network (CNN)
38 CNN :=
39     Repeat{min_repeat, max_repeat}(
40         ConvolutionalLayer(RANGE(in_min, in_max),
41                             RANGE(out_min, out_max)
42                             ,
43                             RANGE(kernel_min,
44                                     kernel_max))
45         -> BatchNorm(num_features)
46         -> CHOICE(Activation)
47         -> PoolingLayer(RANGE(kernel_min,
48                             kernel_max))
49     )
50     -> Flatten()
51     -> Repeat{min_repeat, max_repeat}(
52         LinearLayer(RANGE(in_min, in_max),
53                     RANGE(out_min, out_max),
54                     CHOICE(Activation))
55     )
56
57 // Decision Forest
58 DecisionForest :=
59     DecisionForest(RANGE(n_trees_min,
60                          n_trees_max),
61                    RANGE(depth_min, depth_max))

```

Listing 4: Predefined model templates

In practice, when sampling a model, the system randomly selects one of these templates and instantiates its building blocks by drawing parameter values (e.g., layer widths, kernel sizes, embedding dimensions, number of trees) from the specified ranges. This process yields a rich variety of architectures, while ensuring that the sampled models remain consistent with patterns observed in real-world in-database ML workloads.

N. Synthetic Query Templates

We describe the query templates used to generate training data and evaluation queries. In the MovieLens dataset, we convert the three queries described in Sec. I into templates and pick the seven most voted data science pipelines from Kaggle [98]. In the TPCx-AI [50] dataset, in addition to the tree queries we described in Sec J, we convert the other use cases queries into templates as illustrated in List. 5 and List. 6. The query sampler randomly samples a model architecture and configuration parameters, and randomly samples filters with different selectivity.

```

1 // Template 4: User Rating Prediction for
  Movies

```

```

2 SELECT DNN(process_gender(gender),
  normalize_age(age), normalize_occupation(
  occupation), split_genres(genres))
3 FROM user CROSS JOIN movie
4 [WHERE AGE_FILTER | GENDER_FILTER |
  OCCUPATION_FILTER | GENRE_FILTER];
5
6 // Template 5: User Opinion Prediction (
  Negative/Neutral/Positive)
7 SELECT DNN(user_id, movie_id)
8 FROM user
9 [WHERE AGE_FILTER | GENDER_FILTER |
  OCCUPATION_FILTER | ZIP_CODE_FILTER];
10
11 // Template 6: Recommend Movies to Users via
  SVD
12 SELECT SVD(user_id, movie_id)
13 FROM user CROSS JOIN movie
14 [WHERE AGE_FILTER | GENDER_FILTER |
  OCCUPATION_FILTER | ZIP_CODE_FILTER |
  GENRE_FILTER];
15
16 // Template 7: Rating Prediction with
  Collaborative Filtering
17 SELECT LightFM(user_id, movie_id)
18 FROM user CROSS JOIN movie
19 [WHERE AGE_FILTER | GENDER_FILTER |
  OCCUPATION_FILTER | ZIP_CODE_FILTER |
  GENRE_FILTER];
20
21 // Template 8: Rating Prediction with
  AutoEncoder
22 SELECT AutoEncoder(user_id, movie_id)
23 FROM user
24 [WHERE AGE_FILTER | GENDER_FILTER |
  OCCUPATION_FILTER | ZIP_CODE_FILTER];
25
26 // Template 9: Detect Gender Stereotypes with
  DNN
27 SELECT DNN(prepare_feature(...))
28 FROM ratings JOIN movie ON ratings.movie_id =
  movie.movie_id
29 [WHERE GENRE_FILTER | TIMESTAMP_FILTER];
30
31 // Template 10: Rating Prediction
32 SELECT DNN(movie_id, age, occupation)
33 FROM user CROSS JOIN movie
34 [WHERE AGE_FILTER | GENDER_FILTER |
  OCCUPATION_FILTER | ZIP_CODE_FILTER |
  GENRE_FILTER];

```

Listing 5: Query templates for MovieLens dataset

```

1 // Template 4: Product Rating Prediction with
  SVD
2 SELECT SVD(user_id, product_id)
3 FROM product_rating
4 JOIN product ON productID = p_product_id
5 JOIN customer ON c_customer_sk = userID
6 [WHERE PRODUCT_DEPARTMENT_FILTER |
  CUSTOMER_BIRTH_DATE_FILTER |
  CUSTOMER_BIRTH_COUNTRY_FILTER];
7
8 // Template 5: Spam Review Detection with DNN
9 SELECT DNN(tf_idf_features(text))
10 FROM review_comments
11 [WHERE ID_FILTER];

```

Listing 6: Query templates For TPCx-AI dataset

```

12
13 // Template 6: Classification of Trips with
      DNN/Decision Forest
14 SELECT DNN/DecisionForest(prepare_feature(...)
      )
15 FROM (
16     SELECT o_order_id, department, quantity,
17            SUM(quantity) AS scan_count,
18            MIN(EXTRACT(DOW FROM date)) AS
      weekday
19 FROM tpcxai_order_serving
20 JOIN tpcxai_lineitem_serving ON o_order_id =
      li_order_id
21 JOIN tpcxai_product_serving ON li_product_id
      = p_product_id
22 GROUP BY o_order_id, date, department,
      quantity
23 )
24 [WHERE TIMESTAMP_FILTER | DEPARTMENT_FILTER |
      WEEKDAY_FILTER | PRICE_FILTER |
      QUANTITY_FILTER];
25
26 // Template 7: Fraud Detection
27 SELECT DNN/LogisticRegression(concat(EXTRACT(
      HOUR FROM time)/23, amount/
      transaction_limit))
28 FROM financial_transactions
29 JOIN financial_account ON sender_id =
      fa_customer_sk
30 JOIN customer ON fa_customer_sk =
      c_customer_sk
31 [WHERE TIMESTAMP_FILTER | AMOUNT_FILTER |
      CUSTOMER_BIRTH_INFO_FILTER];
32
33 // Template 8: Sales Prediction
34 SELECT DNN(store_id_encoder(store_id),
      department_encoder(department),
      normalize_week(week))
35 FROM store_dept
36 [WHERE DEPARTMENT_FILTER | WEEK_FILTER |
      STORE_FILTER];
37
38 // Template 9: Customer Segmentation
39 SELECT KMeans/DNN(prepare_feature(...))
40 FROM (
41     SELECT YEAR(date) AS invoice_year,
42            quantity * price AS row_price,
43            or_return_quantity * price AS
      return_row_price
44 FROM order
45 JOIN lineitem ON o_order_id = li_order_id
46 JOIN order_returns ON or_order_id =
      o_order_id
47 JOIN product ON p_product_id = li_product_id
48 )
49 [WHERE DATE_FILTER | STORE_FILTER |
      PRODUCT_FILTER | DEPARTMENT_FILTER];
50
51 // Template 10: Customer Satisfaction
      Prediction
52 SELECT DNN(prepare_feature(...))
53 FROM customer
54 CROSS JOIN product
55 JOIN lineitem ON li_product_id = p_product_id
56 [WHERE CUSTOMER_INFO_FILTER |
      DEPARTMENT_FILTER | PRICE_FILTER];

```